Grb10a knockdown in *Danio rerio* during early life alters growth and cardiometabolic function associated with a remodelled transcriptome

Bridget L Evans[1], Terence Garner[1], Chiara De Leonibus[1], Oliver H Wearing[2], Holly A Shiels[2], Adam F L Hurlstone[3], Peter E Clayton[1], Adam Stevens[1*]

Affiliations:

[1] Division of Developmental Biology and Medicine, School of Medical Sciences, The Faculty of Biology, Medicine, and Health, University of Manchester, Manchester, UK.

[2] Division of Cardiovascular Sciences, School of Medical Sciences, Faculty of Biology Medicine and Health, University of Manchester, Manchester, UK.

[3] Division of Infection, Immunity, and Respiratory Medicine, School of Biological Sciences, Faculty of Biology, Medicine, and Health, University of Manchester, Manchester, UK.

BLE - bridget.evans@postgrad.manchester.ac.uk ORCID 0000-0001-7481-606X

TG - terence.garner@manchester.ac.uk ORCID 0000-0003-3962-9730

CDL - c.deleonibus@tigem.it ORCID 0000-0003-4440-3402

OHW- wearingo@mcmaster.ca ORCID 0000-0002-1866-0416

HAS - holly.shiels@manchester.ac.uk ORCID 0000-0001-5223-5205.

AFLH - adam.hurlstone@manchester.ac.uk ORCID 0000-0001-5260-9457.

PEC - peter.clayton@manchester.ac.uk ORCID 0000-0003-1225-4537.

AS* - adam.stevens@manchester.ac.uk ORCID 0000-0002-1950-7325.

*Corresponding author.

Abstract

Embryonic growth trajectory is a risk factor for chronic metabolic and cardiovascular disorders and influences birth weight along with early post-natal weight gain in humans. Grb10 is a negative regulator of the main pathways driving embryonic growth and knock-out in mammals increases insulin sensitivity and growth trajectory. This study investigates in *Danio rerio* the long-term cardiometabolic consequences and associated transcriptomic profiles of morpholino induced early life disruption of *grb10a* expression. The associated transient knockdown of *grb10a* increased embryonic growth (+7 %) and metabolic rate (+25 %), while decreasing heart rate (-50 %) in early life. Juvenile growth and respiratory rate were also elevated (+30 % and 7-fold increase respectively). This was associated with permanent remodelling of the transcriptional landscape and the dysregulation of multiple growth-related pathways. This study indicates that zebrafish are a suitable model for life-long investigation of the link between early growth and later life disease risk.

35 **Introduction**

36 In humans, small and large for gestational age (SGA, LGA) status, caused by embryonic growth
37 aberration, are early risk factors for chronic metabolic and cardiovascular disorders, such as
38 type II diabetes (TIID), obesity, cardiac dysfunction, and hypertension (1–3). As these
39 disorders are an ever-increasing concern, efforts must be made to identify early risk factors
40 and develop novel therapeutics for prevention and treatment. While this correlation is widely
41 replicated in human populations, targeted in-vivo studies to elucidate this phenomenon and
42 the pathways involved are lacking. The zebrafish is an ideal model organism for longitudinal
43 study owing to its rapid generation time and is also highly suitable for developmental studies
44 as embryos are easily accessible and transparent.

45 Embryonic growth is driven by the insulin/insulin like growth factor (Ins/IGF) signaling
46 pathway (4). Circulating insulin and IGF levels indicate the caloric and nutrient condition of
47 the extrauterine environment and developmental rate positively correlate with Ins/IGF serum
48 levels. Glucose metabolism, glycogen and protein synthesis, as well as proliferation are
49 promoted if the environment is considered favourable (5). Developmental plasticity enables
50 phenotypic alterations to occur in response to fluctuations in the external environment to
51 ensure survival. This is important for healthy development, though phenotypic responses for
52 immediate survival may come at the expense of elevated disease risk in later life. While
53 dysfunction of the Ins/IGF pathway correlates with growth restriction and dysfunctional
54 energy homeostasis (6), SGA and LGA individuals rarely present with mutations in the core
55 pathway, suggesting other factors must be involved in subsequent pathway deregulation.

56 Growth factor receptor bound protein 10 (GRB10) is a negative regulator of the Insulin/IGF
57 signaling pathway. Inhibition by GRB10 downregulates the growth response, promoting a
58 switch from glucose to fat metabolism and halting cell cycle progression (7–9). GRB10
59 expression limits placental growth and efficiency (10) and correlates with small body size (11).
60 In humans, genome wide association studies show *GRB10* is strongly associated with TIID (12),
61 and *GRB10* copy number variation is associated with Silver Russell Syndrome (13), a rare
62 growth disorder typically characterised by intrauterine growth restriction, SGA status,
63 hypoglycemia, poor muscle development, and fat deposition. The role of GRB10 in the
64 regulation of human growth is notably associated with response to recombinant human

growth hormone in children with growth hormone deficiency (14,15). The interaction between the environment and the control of *GRB10* expression has also been investigated, and growth response was shown to be modulated by genotype in association with day length (16). As metabolic and cardiac disorders presenting in adulthood are thought to originate during foetal development (17–19), understanding the impact of altered embryonic growth trajectory on later life disease is important to highlight at-risk individuals.

Moreover, variability in Grb10 expression is also linked to the dramatic range of body sizes observed between cetacean species (20), suggesting that modulating *grb10* expression could be an important target for agri- and aqua-culture. Average daily mass gain is elevated in beef cattle with a *grb10* associated deletion (21), and *grb10* single nucleotide polymorphisms (SNPs) impact muscle and lipid mass, angularity, and body conditioning score (22). Global knockout of *grb10* in mice correlates with elevated muscle mass, reduced lipid mass, and insulin sensitivity (23,24). Therefore, understanding the impact disruptions to early-life growth trajectory have on mature organism size, average daily gain, and lipid to muscle ratio may provide the groundwork to boosting meat yield, and quality which is required to match the growing global demand for protein.

Here, zebrafish (*Danio rerio*) were used to assess the importance of *grb10* as a coordinator of growth, metabolism, and cardiac health, in order to investigate the impact of early-life growth disruption on later-life cardiometabolic phenotype. *Grb10a* was transiently suppressed during zebrafish embryogenesis by antisense oligonucleotide directed blocking of mRNA splicing. *Grb10a* was confirmed to have an impact not only on embryonic growth, but also on cardiac and metabolic phenotypes. Importantly, this impact was found to persist into adulthood, inducing an enduring remodelling of the transcriptomic landscape.

Materials and Methods

Zebrafish Husbandry

AB zebrafish were maintained under standard conditions (≈28 °C; 14 h light/10 h dark cycle; stocking density < 5 fish per litre) within the Biological Services Unit of The University of Manchester. Embryos were collected and raised in egg water (Instant Ocean salt 60 µg/mL) up to 5 days post-fertilisation (dpf) and transferred to the main aquarium system. Young fry were fed powdered food and rotifers, while older fry and adults were fed powdered food and

95 brine shrimp (ZM Fish Food and Equipment, Winchester, UK). All regulated procedures
96 received ethical approval from the Institution's ethical review board and were performed
97 under a Home Office Licence (PPL P005EFE9F9 to HAS).

98 **Transient Knockdown of *grb10a* Expression by Microinjection of Antisense Oligonucleotide**

99 In accordance with current guidelines for morpholino use in zebrafish (25), the use of
100 morpholino-modified antisense oligonucleotides to knockdown (KD) *grb10a* was validated in
101 several ways. Morpholinos targeting two distinct sites should yield a similar phenotype, which
102 should display a dose-response effect and be rescuable by RNA co-injection, and a suitable
103 control morpholino with no phenotypic effect should be used to account for microinjection
104 technique (25). Morpholino-modified antisense oligonucleotides targeting the splice donor
105 sites of zebrafish *grb10a* coding exon three (e3i3) or four (e4i4) were designed by and
106 obtained from Gene Tools, LLC (Philomath, OR, USA) along with a standard control (SC)
107 oligonucleotide targeting human β-globin. Oligonucleotide sequences are listed in Table 1.
108 Microinjection solutions were generated as outlined in Table 2. Concentrations of ingredients
109 were consistent with standard practice (25). Phenol red and n-Cerulean (nuclear-targeting
110 blue fluorescent protein) mRNA were included in each solution to allow monitoring of
111 successful injection. A P-97 Flaming/Brown Micropipette Puller (Sutter Instruments, Novato,
112 CA, USA) was used to generate microinjection needles from 1 mm OD glass capillaries, which
113 were backloaded with 2 µl of injection solution and mounted on a needle holder held in a
114 micromanipulator attached to a PLI-100A Picoliter Injector (Warner Instruments, Hamden,
115 CT, USA). Embryos were injected once, as per established method (25), into the yolk directly
116 below the cell mass. Embryos were injected before the four-cell stage and were screened for
117 fluorescence at 48 hours post fertilisation (hpf) to ensure constitutive and even uptake of the
118 injection material. Non-uniformly or weakly-fluorescent embryos were removed.

119 **Validation of *grb10a* Knockdown by PCR**

120 Primer sequences, outlined in Table 1, were designed using SnapGene® software (GSL
121 Biotech, San Diego, CA, USA; available at snapgene.com) and synthesised by Thermo Fisher
122 Scientific (Waltham, MA, USA). Sequences were designed to be approximately 20 base pairs
123 with a GC content between 40 and 50 % and start with GC or GG to improve target annealing.
124 Primer pairs were designed to anneal at similar temperatures, and specificity was confirmed

125 with Primer BLAST (26). To confirm antisense oligonucleotide activity, RNA was extracted
126 from pooled zebrafish embryos at 24, 48, 72, 96, and 120 hpf (n=3, 5 embryos per pool). RNA
127 extraction was performed using QIAGEN RNeasy lipid extraction kit according to the
128 manufacturer's instructions, and cDNA was generated by reverse transcription using the
129 ProtoScript® II First Strand cDNA Synthesis Kit (NEB). The cDNA was amplified with primers
130 flanking each splice site. PCR was performed using Taq polymerase (New England Biolabs
131 (NEB, Hitchin, UK)) with thermocycling parameters outlined in Table 3. β-actin (*actb1*) was
132 used as a control for cDNA integrity.

133 **Signalling Analysis by Western Blotting**

134 96 hpf zebrafish embryos were deyolked in Ringer's Buffer (n=15, performed in triplicate).
135 Embryos were resuspended in 100 µl RIPA buffer (150 mM NaCl, 1 % Nonident P-40, 0.5 %
136 Sodium deoxycholate, 0.1 % SDS, 25 mM Tris pH 7.4) containing protease and phosphatase
137 inhibitors (Thermo Fisher Scientific) and homogenised by passing through a 22 g needle.
138 Samples were incubated on ice for 30 minutes. The supernatant was clarified by
139 centrifugation at 13000 rpm at 4 °C for 20 minutes and collected. Samples were denatured at
140 98 °C for 5 minutes with an equal volume of Laemmli buffer (final concentration 2 % SDS, 10
141 % glycerol, 60 mM Tris-Cl, 0.01 % bromophenol blue, 0.1 % β-Mercaptoethanol). Proteins
142 were separated on a 10 % SDS acrylamide gel using BioRad Western Blot apparatus and
143 powerpack for one hour at 130 V, 400 mA (running buffer 25 mM Tris, 200 mM glycine, 0.03
144 % SDS). Proteins were transferred for one hour in transfer buffer (25 mM Tris-HCl pH 7.6, 200
145 mM glycine, 20 % methanol, 0.03 % SDS) onto a membrane preactivated in methanol. The
146 membrane was washed three times in TBS-T (137 mM NaCl, 2.7 mM KCl, 19 mM Tris, 0.1 %
147 Tween-20) prior to incubation in blocking buffer (3 % BSA in TBS-T) for one hour. The
148 membrane was rinsed three times in TBS-T and incubated overnight in primary antibody
149 (Table 4) at 4 °C under constant agitation. The membrane was rinsed three times in TBS-T
150 prior to incubation in secondary antibody (Table 4) for one hour at room temperature. The
151 membrane was then covered with ECL Western Blotting Substrate (Promega, Southampton,
152 UK) and imaged immediately using a BioRad ChemiDoc XRS+ Imager. Protein expression was
153 quantified from band intensity in ImageJ (27).

154

155 **Generation of *grb10a* mRNA for Overexpression and Knockdown Rescue**

156 Total RNA was extracted from a pool of 96 hpf zebrafish embryos using QIAGEN RNeasy lipid
157 extraction kit according to the manufacturer's instructions, and cDNA was generated by
158 reverse transcription using the ProtoScript® II First Strand cDNA Synthesis Kit (NEB). *Grb10a*
159 was amplified from cDNA by high specificity PCR (NEB Q5 Hot Start) with primers
160 complimentary to the 5' and 3' ends of the open reading frame (Table 1). The product was
161 purified using QIAGEN Quick Gel Extraction, blunt ligated into pCR-Blunt II-TOPO (Thermo
162 Fisher Scientific) and transformed into *E. coli* following an established protocol. Purified
163 plasmid was sequenced by GATC Biotech Sanger Sequencing to confirm successful cloning.
164 The insert was then liberated by digestion with *Cla* I and *Xba* I restriction enzymes (NEB) and
165 subcloned in pCS2+(28). Capped RNA was generated using the mMESSAGE mMACHINE® SP6
166 Transcription Kit (Thermo Fisher Scientific) according to the manufacturer's instructions.
167 pCS2+ -grb10a was linearised by *Nsi* I (NEB) digestion prior to RNA generation. RNA was
168 purified by MEGAclear™ Transcription Clean-Up. 1 µl of the purified RNA was analysed by gel
169 electrophoresis to confirm amplification and structural integrity.

170 **Physiological and Metabolic Phenotype Measurements**

171 Whole body length, the longest straight-line distance between the snout and tip of the
172 notochord, and yolk area measurements were taken every 24 hours from 48 to 120 hpf (Zeiss
173 Axiocam MRm s1381, Zeiss ZEN lite (2012)). Embryos were dechorionated and acclimatised
174 for ≥ one hour before imaging. Images were imported into ImageJ, which was calibrated with
175 an image of a graticule of known size. Data were imported into GraphPad Prism version 7.00
176 for Windows (GraphPad Software, La Jolla, CA, USA, www.graphpad.com).

177 To investigate embryonic cardiac phenotype, embryos were sedated using a concentration
178 known to have no impact on cardiac function (0.04 % MS-222 solution (29)). Heart beats were
179 counted over a 20 second period and converted to beats per minute (bpm).

180 A Glucose Uptake-Glo TM Assay (Promega) was performed on 96 hpf zebrafish as an index of
181 metabolic rate differences between treatment groups. Individual zebrafish embryos (n=5 per
182 treatment) were injected with 1 mM 2-deoxyglucose-6-phosphate directly into the yolk and
183 allowed to recover for 30 minutes. Embryos were processed in accordance with the
184 manufacturer's instructions. Luminescence was measured on a Synergy™ H1 Microplate

185 reader (BioTek Instruments, Inc., Winooski, VT, USA), software version 2.07.17, with 8
186 readings per well.

187 **Quantitative PCR**

188 Quantitative PCR (qPCR) primers amplifying *grb10a* and markers of cardiac dysfunction were
189 designed (Table 1) and their efficiency validated (30). RNA for comparison of gene expression
190 between SC and KD samples was extracted from pooled (n=10) embryonic zebrafish or pooled
191 (n=3) adult (<1 year) heart samples by QIAGEN RNEasy Lipid Tissue Extraction kit according to
192 the manufacturer's instructions. Samples were repeated in triplicate and tested for gene
193 expression by qPCR (Applied Biosystems Power SyBr Green) (Table 3). Results were visualised
194 using MxPro QPCR Software (Agilent, Santa Clara, CA, USA). Relative fold change in gene
195 expression was calculated using the ΔΔCt method according to the following equation:

196 $$\Delta\Delta Ct = \Delta Ct_{e3i3} - \Delta Ct_{SC}$$

197 where

198 $$\Delta Ct = Ct_{gene\ of\ interest} - Ct_{housekeeping\ gene}$$

199 and

200 $$Fold\ change = 2^{-\Delta\Delta Ct}$$

201 Data were imported into GraphPad and unpaired t-tests were used to assess the difference
202 between samples.

203 **Transcriptomic Analysis**

204 Temporal changes in gene expression were assessed by computational analysis of
205 transcriptomic data. Pooled samples (n=5) were generated from each treatment group (SC,
206 KD) at 5, 10, 15, 20, and 30 dpf, with three repeats per sample. Individuals were culled under
207 terminal anaesthesia with only tissue anterior to the gills included, and total RNA was
208 prepared. Transcriptomic data were generated using Affymetrix Zebgene 1.0st arrays. Data
209 for all 75212 gene probes were imported into Qlucore Omics Explorer 2.2 (Lund, Sweden) as
210 .cel files and normalised using the robust multi-array average (RMA) approach with a gene
211 level summary. Zebrafish gene identities were assigned using the Affymetrix gene definitions.

212 Human orthologues were mapped (GRCh 38) using the *biomaRt* R-package (31). A workflow
213 pipeline of the subsequent transcriptomic analyses is outlined in *Supplementary Figure 1*.

214 Unsupervised analysis of gene expression by age group was conducted by generating
215 hierarchically clustered heat maps. Standard deviation filtering (standard deviation of specific
216 gene expression divided by maximum gene standard deviation $[s/s_{\max}]$) was performed on
217 the dataset to remove genes with low variance, unlikely to be informative (or below
218 detectable levels). The projection score (32), was used to determine the threshold for filtering
219 by calculating the maximum separation present in principal component analysis (PCA).

220 **Hypernetwork Modelling**

221 Hypernetwork analysis was performed to model the dynamics of the transcriptome by
222 quantifying shared correlations between target genes, a general model of which is outlined
223 in *Supplementary Figure 1*. All analyses were performed in R (version 3.4.2).

224 Using samples from all time-points in either SC (n=15) or KD (n=15) fish, Pearson's correlation
225 coefficients (*r*) were calculated between genes identified by unsupervised analysis (g) [KD =
226 119, SC = 297] and the rest of the transcriptome (g^c) [KD = 75093, SC= 74915]. Positive and
227 negative correlations greater than ± 1 standard deviation (sd) from the mean of the R-values
228 were binarized separately and the resulting matrices combined. In this way, a matrix (*M*) was
229 formed describing the positive and negative correlates of each element (∈) of *g* separately:

230 $$\in \text{ of } g \text{ in } M = \begin{cases} 1, & x > \pm 1sd|r| \\ 0, & x \geq \text{otherwise.} \end{cases}$$

231 The resulting binary matrix (M) was multiplied by its transpose (M^t) to generate a matrix
232 ($M.M^t$) which lists the number of shared correlations between any pair of genes (g). This
233 matrix represents the hypernetwork describing the higher order relationships between genes
234 not represented in traditional transcriptomic approaches. This measurement of co-ordination
235 has been hypothesised to model functional relationships (33). Coordination between genes
236 with age-related expression and the rest of transcriptome was determined using the Galois
237 correspondence. This was represented by the subset of the transcriptome ($\subset g^c$) showing
238 correlated expression with all the transcripts from the hypernetwork cluster ($\subset g$).

239

240 **Quantification of Network Topology**

241 Correlation networks model functional relationships within gene networks (34) and allow
242 identification of clusters of highly connected genes (35). Quantification of SC and KD
243 hypernetwork properties (connectivity and entropy) was performed on the matrix $M.M^t$.
244 Connectivity is defined here as the sum of connections shared by each element of the network
245 (g) and measures the direct and indirect relationships between them.

246 Entropy describes the degree of disorder within the distribution of shared correlations
247 measured in each element of g. Entropy is correlated with the differentiation potential of a
248 cell (36), with low entropy indicating specific pathway activation and high entropy indicating
249 high signalling pathway redundancy. Entropy has also been used as an index of regularity and
250 patterning (37). Entropy was measured using R package BioQC (38).

251 As the hypernetworks formed three clusters of genes when clustered hierarchically, all
252 following analysis focused on the 20-30 dpf cluster (86 SC genes, 67 KD genes). Clusters were
253 isolated and within-cluster connectivity and entropy were calculated per gene.

254 The expected background connectivity and entropy were measured in 1000 iterated
255 hypernetworks using randomly selected genes (86 random genes and 67 random genes for
256 the SC and KD respectively) (*Supplementary Figure 2*). The median expected connectivity and
257 entropy were subtracted from the experimentally derived values to control for the
258 background. Experimental data for SC and KD zebrafish are therefore presented as the
259 difference between expected and observed connectivity and entropy.

260 **Gene Ontology**

261 To associate gene expression with biological processes, gene set enrichment analysis (GSEA)
262 was performed (39). Unsupervised analysis was supported with GSEA ranked by age group
263 ANOVA false discovery rate modified p-values [q-values] (Qlucore) using genes mapped to
264 human orthologs. GSEA was also performed on regression data (ranked by R-value) using
265 Webgestalt (40). Over-representation analysis (ORA) was used to identify gene ontology
266 associated with unranked gene sets (Webgestalt). All gene ontology analysis used the GO
267 Biological Process Ontology gene list (Molecular Signatures Database (39,41)).

268

269 **Oxygen Consumption as a Measure of Metabolic Rate**

270 To analyse metabolic rate, oxygen consumption was measured in 30 dpf zebrafish from each
271 treatment group. Individual zebrafish were placed into 1 of 4 stop-flow respirometry
272 chambers (volume 2 ml) and allowed to acclimate at 28 °C for > one hour. Chambers were
273 refreshed immediately prior to the experiment until oxygen saturation measured 100 %.
274 Optical oxygen sensors paired with oxygen sensor spots (Pyroscience, Aachen, Germany)
275 were used to measure oxygen saturation within the chambers and recorded using a
276 FireStingO2 Fiber-optic oxygen and temperature meter. Temperature was maintained at 28 ±
277 0.3 °C and was monitored and recorded with the FireSting integrated temperature meter.
278 Probes were calibrated according to the manufacturer's instructions. Chambers were
279 randomised per trial, with one chamber left empty to correct for background bacterial
280 respiration. Oxygen consumption over time curves were recorded in triplicate with five trials
281 per treatment. Chambers were refreshed when oxygen saturation reached 80 %. Oxygen
282 consumption was measured as the change in oxygen saturation within the chamber per trial.
283 To calculate the rate of oxygen consumption, linear regression in Microsoft Excel was used to
284 approximate the change in oxygen saturation during each trial. This was normalised against
285 the dry mass of the subject, length of the trial, and volume of the respirometry chamber
286 according to the following equation:

287 $$Oxygen\ consumption\ (\mu g O_2 h^{-1} g^{-1}) = \frac{\Delta O2\% \times \frac{7900 \mu g L^{-1}}{100} \times\ chamber\ volume\ (L)}{time\ (h)\ \times\ mass\ (g)}$$

288

289 Where 7900 μgL^{-1} is equivalent to 100 % oxygen saturation at 28 °C. This normalises the data
290 against the dry mass of the subject, time of the trial, and volume of the respirometry chamber.

291 **Statistical Tests**

292 For transcriptomic analyses, rank regression (least squares method) was used to generate the
293 most appropriate linear model for each probe (the smallest degree of variance over the
294 sample). Multi group analysis of variance (ANOVA) was used to associate each gene ID with
295 time dependent gene expression. Wilcoxon rank sum test (ggpubR package for R (42)) was
296 used to test for differences of network topology between groups. False discovery rate (FDR)

297 adjustment was made using the Benjamini-Hochberg method and applied to the gene
298 expression and ontology analysis (43).

299 All data were ROUT tested (44) for outliers and subject to D'Agostino and Pearson normality
300 tests. All comparisons between SC and KD measurements were performed using an unpaired
301 t-test. Comparisons of multiple groups were performed using one-way ANOVAs. Post-hoc
302 power calculations were performed to confirm sample sizes were sufficient, where $\alpha = 0.05$.

303 **Results**

304 **Knockdown of *grb10a* Expression by Splice-Blocking Antisense Oligonucleotide**

305 As *grb10* has been linked to embryonic growth trajectory, expression was examined over the
306 first 120 hpf (hours post fertilisation) in zebrafish embryos. qPCR analysis of *grb10a*
307 expression at 24-hour intervals revealed a strong upregulation at 48 hpf compared to
308 housekeeping genes (*Figure 1a*). Expression of the *grb10* paralogue, *grb10b*, was not
309 detectable at any time point.

310 To manipulate the expression of *grb10a*, zygotes were microinjected with splice-blocking
311 antisense oligonucleotides: e3i3 and e4i4. Two distinct splice sites, exon 3 and 4 donor splice
312 sites (*Figure 1b*), were targeted in order to confirm the specificity of phenotypes
313 accompanying oligonucleotide injection, in accordance with current guidelines (25).
314 Disruption of the targeted splice site was confirmed through multiplexed RT-PCR
315 amplification using a mixture of primers (F, R1 and R2) flanking the splice sites (*Figure 1b*). No
316 products at all were detected for standard control oligonucleotide injected embryos and only
317 a single product of the anticipated size was detected for embryos injected with either e3i3 or
318 e4i4 (*Figure 1c*), consistent with amplification from a cDNA rather than genomic DNA
319 template. Further, the corresponding intron was shown by sequencing to be included in the
320 transcript for e3i3 and e4i4 treated zebrafish (data not shown).

321 To address the effect of *grb10a* KD on insulin signalling, phosphorylation of key proteins in
322 the insulin signalling pathway was analysed by Western blotting. As shown in *Figure 1d*,
323 phosphorylated (active) versus total protein ratios of AKT, ERK, and S6 were significantly
324 elevated in *grb10a* KD zebrafish at 96 hpf compared to SC ($p=0.0080$, 0.0497, <0.0001
325 respectively, $n=3$), with S6 activation almost 5 times greater in KD zebrafish compared to SC.

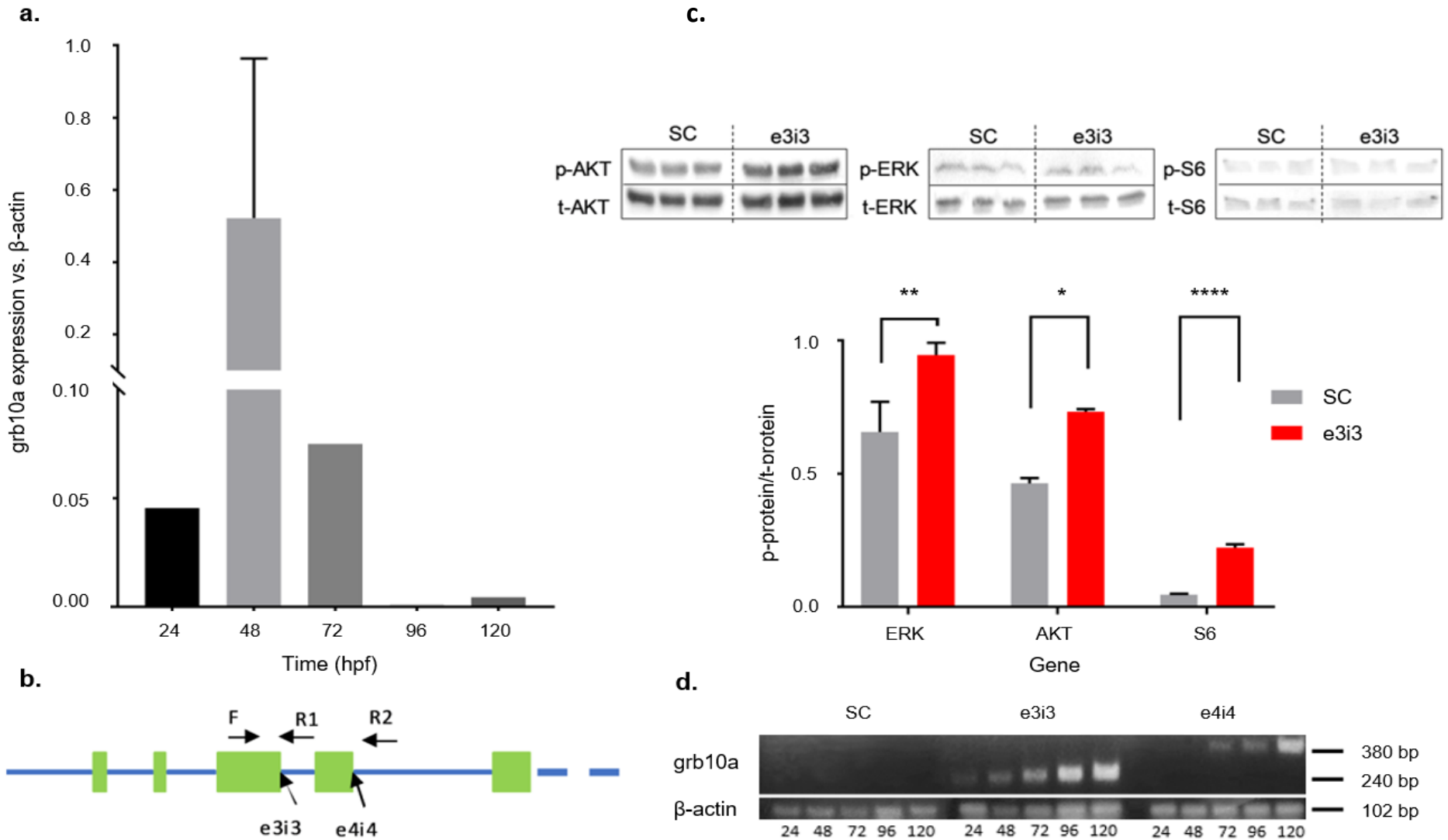

Figure 1:* Grb10a *is successfully knocked down in zebrafish injected with splice-blocking antisense oligonucleotides. 1a. *Grb10a* qPCR of WT embryos (24-120 hpf, triplicated, n=5 per well). Data is shown as gene expression relative to β-actin and shows a significant peak at 48 hpf. ***1b.*** Schematic of the first five exons of the zebrafish *grb10a* gene. 5' splice sites are highlighted with the forward and reverse primer triad indicated. ***1c.*** PCR amplification of the e3i3 and e4i4 splice site in embryos treated with either Standard Control morpholino, e3i3, or e4i4 (24-120hpf, n=5 per well). β-actin was used as a positive control. ***1d.*** Western blot results of phosphorylated vs total protein ratios for three major signalling molecules of the insulin signalling pathway: ERK, AKT, and S6. Activation of all three proteins was found to be significantly elevated in KD zebrafish compared to SC (n=3, unpaired t-test **=0.0083, *=0.0498, ****<0.0001).

332 **Growth Trajectory and Early Life Cardiometabolic Phenotype is Significantly Impacted by**
333 **Transient *grb10a* Perturbation**

334 To determine the effect of *grb10a* KD on embryonic growth, total body length was measured
335 in antisense oligonucleotide injected animals at various timepoints. *Figure 2a* shows that
336 initially, total body length was comparable between KD and SC zebrafish (2.857 ± 0.0549 mm
337 vs 2.826 ± 0.0962 mm, p=0.7896, n=9 and n=10 respectively). From 48 hpf, corresponding to
338 the peak in WT *grb10a* expression (*Figure 1a*), KD zebrafish began to diverge from SC
339 individuals. Body length was significantly different between the two groups, with KD zebrafish
340 longer on average than SC zebrafish (3.411 ± 0.0165 mm vs 3.177 ± 0.0231 mm at 72 hpf,
341 p<0.0001, n=46 and n=41 respectively). This phenotype was reversed in zebrafish
342 overexpressing *grb10a,* with individuals injected with *grb10a* mRNA significantly shorter than
343 SC counterparts (3.361 ± 0.0239 mm vs 3.505 ± 0.0339, p=0.001, n=24 and n=25 respectively),
344 as shown in *Figure 2b*. Co-injection of e3i3 and *grb10a* RNA resulted in normalisation of
345 growth (3.505 ± 0.0339 mm vs 3.564 ± 0.0265 mm, p=0.3792, n=25), confirming the validity
346 of e3i3 induced *grb10a* KD. Moreover, *grb10a* KD induced by e4i4 (albeit weaker than e3i3;
347 *Figure 2c*) also resulted in increased body length; while the ability of *grb10a* overexpression
348 to suppress growth was shown to be dose dependent (*Figure 2c*). Intriguingly, by 120 hpf body
349 length converged for both KD and OE, indicating activation of compensation to regulate
350 growth.

351 Embryonic heart rate was measured to investigate the impact of *grb10a* KD on
352 cardiometabolic phenotype. As shown in *Figure 2d*, average heart rate began to diverge
353 between the treatment groups at 48 hpf, correlating with the WT peak in *grb10a* expression.
354 While heart rate increased slightly over time in SC zebrafish, in-line with increasing body size,
355 average KD heart rate fell. By 120 hpf, average heart rate for KD individuals was almost 50 %
356 lower than SC individuals (61.5 ± 6.97 bpm vs 118.4 ± 2.83 bpm, p<0.0001, n=14 and n=19
357 respectively).

358 Embryonic metabolic rate was also investigated in KD and SC zebrafish by looking at yolk
359 absorption. The reduction in yolk area over time was measured to evaluate the difference in
360 the rate of yolk consumption between treatment groups. As shown in *Figure 2e*, there was no
361 significant difference between yolk areas at 24 hpf (p=0.8185, n=10). Yolk area declined
362 steadily from 48 hpf, and significantly more so in KD zebrafish compared to SC zebrafish for

363 the remaining period of observation (0.298 ± 0.0055 mm^2 vs 0.390 ± 0.0104 mm^2, $p<0.0001$,
364 n=18 and n=19 respectively). This suggested that metabolic rate was elevated in KD zebrafish
365 compared to SC. To further interrogate insulin signalling, a Glucose Uptake-Glo™ Assay was
366 performed to monitor 2-deoxyglucose-6-phosphate accumulation and support these findings.
367 As shown in *Figure 2f*, 2D6P accumulation was significantly higher in KD zebrafish compared
368 to SC, an increase of almost 30 % (p=0.0002, n=5). These findings are consistent with the role
369 of *grb10a* as a negative regulator of the insulin signalling pathway (5).

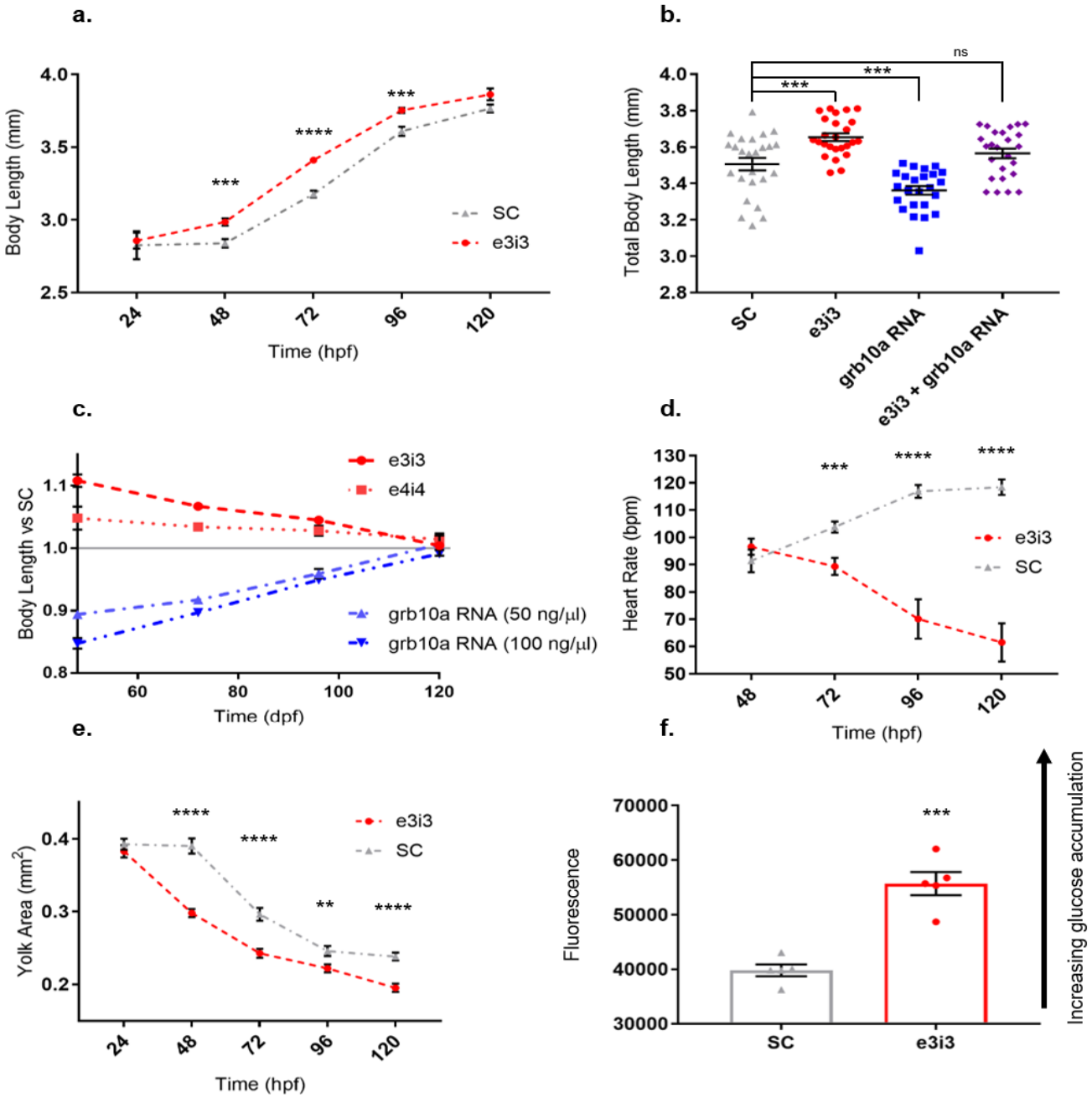

Figure 2: Growth and cardiometabolic phenotype are significantly impacted by* grb10a *perturbation. 2a. Mean total body length ± SEM of SC and KD zebrafish from 24 to 120 hpf. T-test significance ***=0.0006 ****<0.0001 ***=0.0001. ***2b.*** Mean total body length ± SEM and individual data points of 96 hpf zebrafish embryos (n=25). *Grb10a* KD phenotype was reversed in *grb10a* overexpression zebrafish. Coinjection resulted in phenotype rescue. One-way ANOVA revealed KD zebrafish were significantly longer, while *grb10a* overexpression zebrafish were significantly smaller than SC (***=0.0001). Rescue zebrafish were of similar length to SC (ns=0.3792). ***2c.*** Mean body length measurements relative to SC ± SEM. E3i3 and e4i4 both exhibit a propensity to elevate body length, while *grb10a* RNA shows a dose-dependent ability to inhibit body length. ***2d.*** Mean heart rate ± SEM in beats per minute of SC and KD zebrafish. Heart rate was significantly lower in KD embryos compared with SC after 48 hpf (***=0.0006, ****<0.0001). ***2e.*** Mean yolk area ± SEM of SC and KD embryos over the embryonic life stage. Following the initial 24 hours, KD zebrafish had significantly smaller yolks compared to SC, indicating yolk content was metabolised at a much higher rate (**=0.0084 ****<0.0001). ***2f.*** Glucose Uptake-Glo™ Assay of 96hpf KD and SC zebrafish, where higher luminescence indicates a greater accumulation of intracellular 2D6P. Luminescence was approximately 30 % greater in KD zebrafish compared to SC (***=0.0002). All SC vs KD comparisons by unpaired t-test.

385 **Transient *grb10a* Knockdown Dysregulates Age-Related Expression in the Transcriptome**

386 To understand whether disruption in embryonic growth trajectory could lead to lasting
387 changes in gene expression, the transcriptomic landscape of SC and KD zebrafish was
388 investigated over the first 30 dpf. As described in the methods, unsupervised hierarchical
389 clustering, standard deviation filtering, and maximised projection scores were used to define
390 a gene set with strong age-associated expression in the SC zebrafish (297 genes with a
391 maximised projection score [PS] = 0.43).

392 Clear age-related associations were identified in the SC transcriptome, with genes falling into
393 four clusters (5 dpf - 163 genes, 10 dpf- 15 genes, 15 dpf – 32 genes, and 20-30 dpf – 87 genes)
394 (*Figure 3a*). Clustering of these same genes was disrupted in the KD zebrafish (*Figure 3b*).
395 Three of the four clusters defined in the controls mapped to the same age-associated cluster
396 in the KD data (10 dpf – 14/15 genes, 15 dpf - 29/32 genes, and 20-30 dpf – 74/87 genes).
397 However, genes associated with 5 dpf expression in the SC zebrafish were generally expressed
398 at different time points in the KD zebrafish (dotted white lines, *Figure 3a* and *Figure 3b*), with
399 a mapping of only 38/163 genes (23%). Notably, 5 genes associated with 5 dpf in SC zebrafish
400 mapped to 20-30 dpf in the KD zebrafish. Human orthologs of these dysregulated genes
401 included *DGAT2* (fatty acid metabolism enzyme), *GAMT* (an enzyme involved in creatine
402 production, required for energy storage, muscle contraction, and fatty acid oxidation), and
403 *PDIA2* (an enzyme involved in thiol-disulphide interchange reactions, particularly in the
404 pancreas).

405 The existence of a pattern of gene expression associated with age in SC zebrafish which is
406 dysregulated in KD zebrafish implies the co-ordination of an altered set of genes in KD
407 animals. In the KD, unsupervised analysis defined a set of 119 genes (maximised projection
408 score = 0.37) which divided into three clusters, only loosely age-associated (5-15 dpf – 37
409 genes, 15-30 dpf – 16 genes and 20-30 dpf – 66 genes) (*Figure 3c*). There was a 90 gene
410 overlap in age-associated genes between the SC and the KD. A further 207 genes were age-
411 associated in the SC and 29 in the KD (*Figure 3d*).

412 Gene set enrichment analysis on the age-related genes in both SC and KD zebrafish
413 demonstrated a range of similar (*Supplemental Table 1*) and dissimilar pathways (*Figure 3e*).
414 This analysis revealed that a range of pathways involving actin and collagen, along with

415 extracellular structure and RNA processing, were co-ordinated in an age-related manner in
416 KD but not SC zebrafish. Also, a set of metabolic pathways were age associated in SC zebrafish
417 but not in KD animals. This clear dysregulation of age-related gene expression in the KD
418 zebrafish implies transient *grb10a* KD induces persistent remodelling of the transcriptome.

419

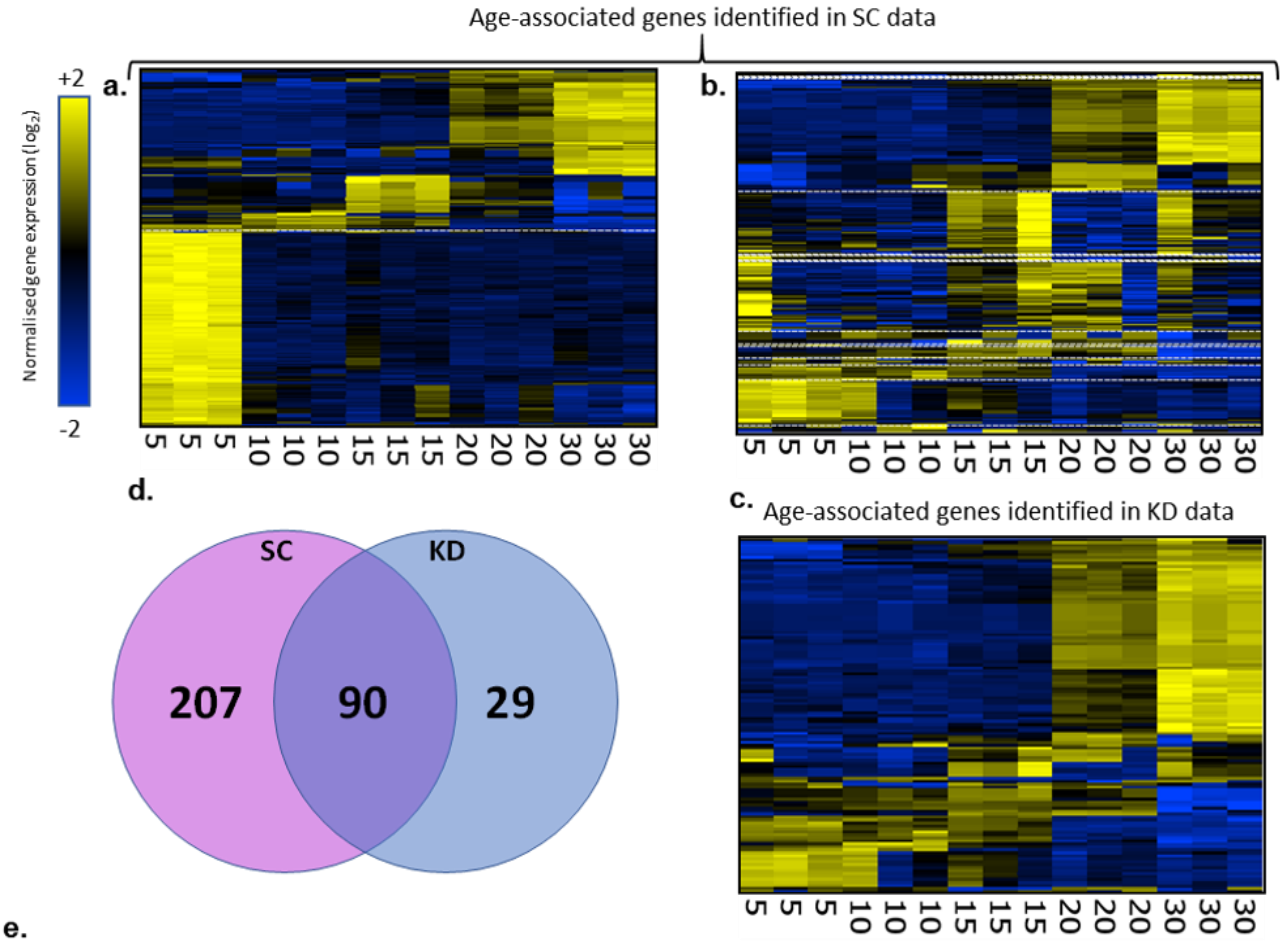

Name	KD NES	KD q	SC NES	SC q
ACTIN FILAMENT BASED MOVEMENT	2.088	0.012	2.176	1.000
PLATELET ACTIVATION	2.068	0.013	2.236	1.000
EXTRACELLULAR STRUCTURE ORGANIZATION	2.011	0.013	2.246	1.000
COLLAGEN FIBRIL ORGANIZATION	2.026	0.014	2.257	1.000
REGULATION OF RNA SPLICING	1.608	0.039	0.726	0.855
GLUTATHIONE METABOLIC PROCESS	1.660	0.031	0.735	0.848
RIBOSOME ASSEMBLY	1.700	0.026	0.743	0.840
REGULATION OF MRNA PROCESSING	1.609	0.039	0.810	0.772
PLATELET DEGRANULATION	1.753	0.022	2.155	0.757
METANEPHROS DEVELOPMENT	1.709	0.026	0.841	0.733
DICARBOXYLIC ACID TRANSPORT	0.690	0.895	1.693	0.048
POSITIVE REGULATION OF WOUND HEALING	0.876	0.703	1.672	0.048
FAT SOLUBLE VITAMIN METABOLIC PROCESS	0.950	0.597	1.655	0.049
POSITIVE REGULATION OF SMOOTH MUSCLE CELL PROLIFERATION	0.986	0.543	1.708	0.048
REGULATION OF STEROL TRANSPORT	1.012	0.503	1.704	0.049
POSITIVE REGULATION OF PROTEIN BINDING	1.033	0.471	1.663	0.049
AMINO ACID TRANSPORT	1.037	0.466	1.703	0.048
POSITIVE REGULATION OF LIPID LOCALIZATION	1.059	0.436	1.757	0.050
CELLULAR MODIFIED AMINO ACID BIOSYNTHETIC PROCESS	1.068	0.423	1.664	0.049
NEGATIVE REGULATION OF EXTRINSIC APOPTOTIC SIGNALING PATHWAY	1.097	0.383	1.674	0.049

Figure 3. Transcriptomic analysis of Standard Control and grb10a Knockdown gene expression over the first 30 dpf. Hierarchically clustered heat maps of gene expression generated from an Affymetrix GeneChip™ Zebrafish Genome Array of SC (***3a***) and KD (***3b*** and ***3c***) zebrafish RNA, taken at 5, 10, 15, 20, and 30 dpf. Expression segregates into three clusters in SC zebrafish (***3a***). Clustering of the same genes identified in ***3a*** are disrupted in the KD dataset (***3b***). Analysing the KD dataset independently shows age-related hierarchical gene expression in the falls into two clusters (***3c***). ***3d***. Venn diagram of age associated genes. ***3e***. Gene set enrichment analysis, using the GO Biological Process Ontology gene list, of the age-related genes in the SC and KD datasets.

427 The top 20 most enriched pathways with differential expression are included here, with associated normalised
428 enrichment scores and q-values.

429 **Transient *grb10a* Knockdown Alters Co-Ordination Within the Transcriptome**

430 To investigate the co-ordination of the transcriptome with age-associated gene expression,
431 hypernetwork models were constructed for the SC and KD datasets based around genes
432 identified by the previous unsupervised analysis. This approach can be used to model
433 functional relationships (33). The outputs of these analyses were visualised as heatmaps
434 where colour intensity represented the number of shared interactions between a gene pair.
435 In SC animals, three clusters of shared interactions were defined. Cluster 1 corresponded to
436 genes expressed at 5 dpf (161/297 genes), cluster 2 at 10 and 15 dpf (50/297 genes) and
437 cluster 3 at 20 and 30 dpf (86/297 genes) (*Figure 4a*). In KD animals, however, only two
438 clusters were identified. Genes in cluster 1 were expressed across 5, 10 and 15 dpf (31/119
439 genes) and genes in cluster 2 expressed at 20 and 30 dpf (65/119 genes) (*Figure 4b*). Notably,
440 the large cluster of co-ordinated interactions at 5 dpf in the SC was entirely absent in the KD,
441 instead forming a new cluster along with genes expressed at 10 and 15 dpf. The 20 and 30 dpf
442 cluster represented 28.9% and 54.6% of the total gene set in the SC and KD zebrafish
443 respectively, indicating a *grb10a* KD-induced remodelling of the transcriptome in later life.

444 Differences in the co-ordination of the transcriptome in later life were quantified using two
445 network topology parameters, connectivity and entropy. Hypernetwork connectivity
446 quantifies the number of interactions within the transcriptome and is related to function.
447 Entropy is a measure of information content and can be thought of as a measure of
448 "disorder"; a decreased entropy (more order) describes a network with little crosstalk and a
449 more discrete function (36,45). While conversely an increased entropy has less order and
450 describes a network with increased crosstalk and pleiotropic function.

451 Changes in connectivity (*Figure 4c*) and entropy (*Figure 4d*) were calculated for genes
452 identified as active at 20-30 dpf by the unsupervised and hypernetwork approaches. This was
453 compared with entropy and connectivity calculations from a thousand iterations of random
454 genes in order to account for random chance (*Supplemental Figure 2*). Genes associated with
455 20-30 dpf in the KD animals were found to be more highly connected and more entropic than

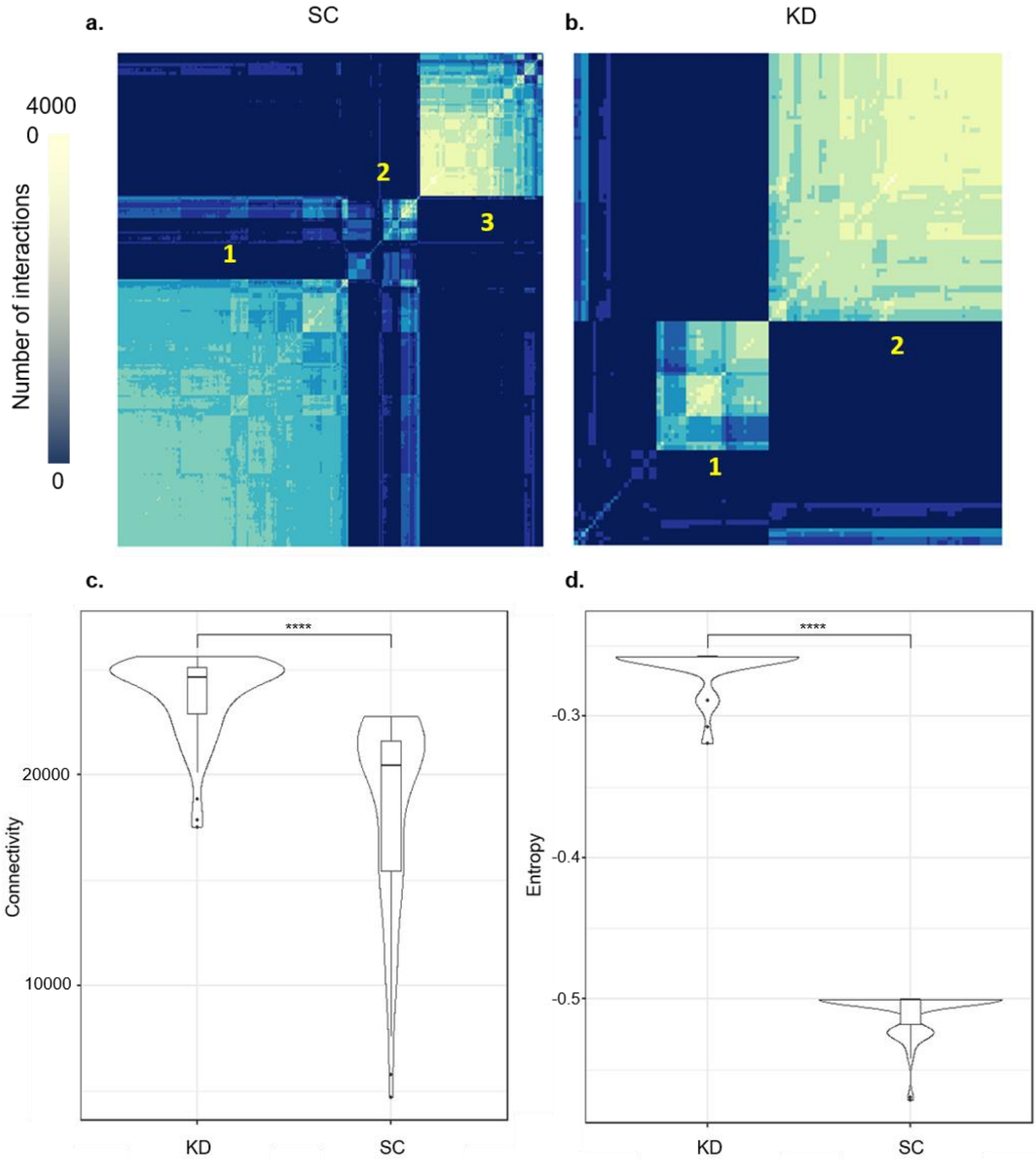

456 ***Figure 4 Coordination within the transcriptome is altered by grb10a KD, as assessed by hypernetwork analysis***
457 ***4a.*** Hypernetwork analysis defined three clusters of highly connected genes in Standard Control zebrafish,
458 corresponding to 5 dpf, 10-15 dpf, and 20-30 dpf respectively. ***4b***. Two clusters were defined in the KD data,
459 corresponding to 5-15 dpf and 20-30 dpf. ***4c*** *and* ***4d***. Violin plots of connectivity (left) and entropy (right) in the
460 20-30 dpf cluster. Both connectivity and entropy were elevated in the KD zebrafish compared to standard
461 controls when controlled for random gene measurements, suggesting more diverse functions.

462 in the SC when normalised for random effects. Additionally, this increase in connectivity is
463 greater (1.20-fold, $p < 1x10^{-6}$) and the reduction in entropy is smaller (2.0-fold, $p < 1x10^{-6}$) in
464 the KD zebrafish compared to the SC in relation to randomly selected gene sets (*Supplemental*
465 *Figure 2*). This assessment of hypernetwork topology demonstrates the co-ordination of age-
466 related gene expression in the SC and the dysregulation in the KD zebrafish. These data show
467 that transient *grb10* KD induces significant remodelling of the transcriptome, enduring in later
468 life, with increased connectivity between genes and a more directed functionality.

469 **Transcriptome-Wide Links to the Enduring Remodelling of Gene Expression Associated**
470 **with Transient *grb10a* Knockdown**

471 Having identified age-related gene expression we now wanted to define a wider set of
472 associated genes which coordinate with age-related gene expression defined by calculating
473 Galois correspondences (the one-to-one correspondence between age-related genes and
474 their correlates).

475 12775 and 459 genes were defined in the Galois correspondence from the 20-30 dpf KD and
476 SC hypernetwork clusters, respectively. 27.8-fold more genes with co-ordinated regulation at
477 20-30 dpf exist in the KD set than SC zebrafish. All genes in the Galois correspondence
478 demonstrated significant rank regression with age (*Supplemental Table 2*). In the KD
479 zebrafish, 7493 genes positively correlate with age (*Figure 5a*), while 5282 negatively
480 correlate (*Figure 5b*). This was reduced to 313 positive and 146 negative co-ordinated genes
481 in the SC. The overlap was 244 (77.9% of SC) and 60 (41.1% of SC) in the positively and
482 negatively correlated sets, respectively. Thus, genes in the Galois correspondence with
483 expression at 20-30 dpf in SC zebrafish demonstrated a similar pattern of expression in KD
484 (*Figure 5c*). However, genes with co-ordinated expression at 20-30 dpf in the KD zebrafish
485 were dysregulated in the SC animals (*Figure 5d*).

486 Gene ontology associated with the 20-30 dpf co-ordinated gene expression clusters in both
487 KD and SC zebrafish (GSEA ranked by R-value, top 100 pathways with weighted set cover) are
488 outlined in *Figure 5e* and *Figure 5f*. A distinctly different set of regulated pathways was noted
489 between the groups. The KD gene set was associated with RNA processing, a range of
490 metabolic pathways, and cardiovascular system development. The SC gene set was associated
491 with growth and immune pathways.

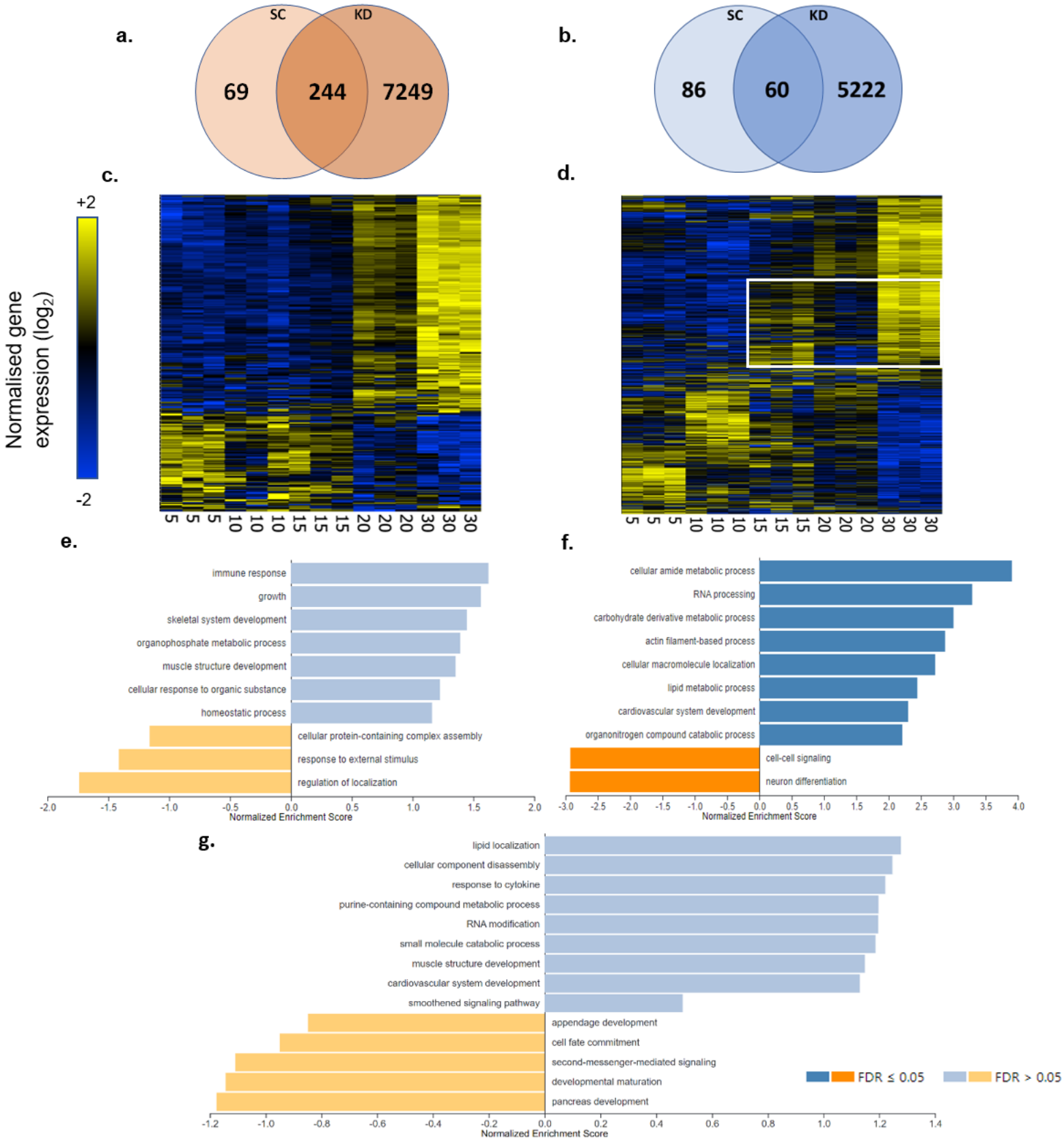

Figure 5 Analysis of the set of genes in the Galois correspondence shows a 27.8-fold increase in the KD ZF. ***5a-5b****.* Venn diagrams of genes positively (left) and negatively (right) correlating with age. ***5c-5d***. Hierarchically clustered heat maps of gene expression of the genes identified in the Galois correspondence. Gene expression in the standard control (***5c***) cluster into two age related groups, whereas expression in the knockdown (***5d***) show significant dysregulation. ***5e-5f*** Gene set enrichment analysis (GSEA) ranked by R-value of rank age regression in the standard control (***5e***) and knockdown (***5f***) Galois correspondence. ***5g*** GSEA ranked by R-value of rank age regression of the cluster of genes in the white box in ***5d***.

499 Of the genes with co-ordinated expression at 20-30 dpf in the KD zebrafish that were
500 dysregulated in the SC animals (*Figure 5d*), there was a subgroup with a distinct pattern of
501 expression at day 15, downregulation at day 20, and re-expression at day 30 (white box,
502 *Figure 5d*). This subgroup of 3460 genes (*Supplemental Table 3*) was associated with a range
503 of gene ontologies related to metabolism and development (*Figure 5g*) and is linked to the
504 spike in growth identified in *Figure 6a*. Pathways included those involved in cardiovascular
505 system development, muscle structure development, and developmental maturation.

506 **The Impact of Transient *grb10a* KD Persists into Adulthood**

507 As dysregulation of pathways associated with growth, cardiovascular system development
508 and metabolism were identified, associated with persistent long-term changes in the
509 transcriptome relating to *grb10a* KD, investigation was conducted into the differences in
510 growth rate, oxygen consumption, and cardiac molecular phenotype in older animals.

511 Total body length measurements were taken up to 30 dpf. As shown in *Figure 6a*, growth was
512 significantly elevated in KD zebrafish compared to SC zebrafish between 15 and 20 dpf (30 %
513 increase, 7.493 ± 0.2726 mm vs 4.320 ± 0.1594 mm, $p < 0.0001$, n=10). This period of change
514 in growth rate corresponded precisely to the cluster of dysregulated genes identified in the
515 KD animals (*Figure 5g*). The growth profile of the KD zebrafish is shifted to an earlier age
516 compared to the SC growth profile, suggesting a faster rate of maturation. The GSEA
517 highlighted a reduction in activity in developmental maturation pathways (normalised
518 enrichment score [NES] < 1) in the controls vs. the KDs, which was replicated in the
519 comparison between KD and SC growth rates at approximately 20 dpf.

520 Juvenile (30 dpf) metabolic rate was investigated by stop-flow respirometry. As shown in
521 *Figure 6b*, oxygen consumption was 7 times greater in KD zebrafish than SC (134.4 ± 15.60
522 $\mu gO_2h^{-1}g^{-1}$ vs 19.0 ± 3.28 $\mu gO_2h^{-1}g^{-1}$, $p<0.0001$, n=5), suggesting metabolic rate was also
523 significantly elevated. Thus, along with significant alteration in gene expression revealed by
524 transcriptomic analysis over juvenile phases, growth and metabolic rates were also divergent.

525 To address whether differences in earlier life course phases might impact adult phenotypes,
526 the impact of transient *grb10a* KD on adult (1 year) cardiac health was assessed by qPCR. As
527 shown in *Figure 6c*, *myl7* expression (an index of muscle mass and hypertrophy) was over 20
528 % greater in KD zebrafish cardiac tissue compared to SC ($p<0.0001$, n=3), while *nppa*

529 expression (cardiovascular homeostasis, associated with atrial fibrillation (46)) was down
530 almost 40% compared to SC zebrafish (p=0.0012, n=3). This not only suggests a protective
531 phenotype in terms of cardiac health, but also highlights the lasting impact of transient
532 *grb10a* KD in adult tissue. There was no difference in the expression of *pcna* (proliferating cell
533 nuclear antigen, an index of cellular proliferation), indicating there was no increase in
534 proliferation. The greater degree of *myl7* expression in the absence of an increase in *pcna*
535 expression suggests an increase in hypertrophy (muscle size) rather than hyperplasia (cell
536 number) in the cardiac tissue.

537 None of these cardiac phenotype marker genes were present in the Galois correspondence
538 associated with persistent alteration of the transcriptome. However, all these genes showed
539 dysregulated expression in the KD animals in early life (*Supplemental Table 4*).

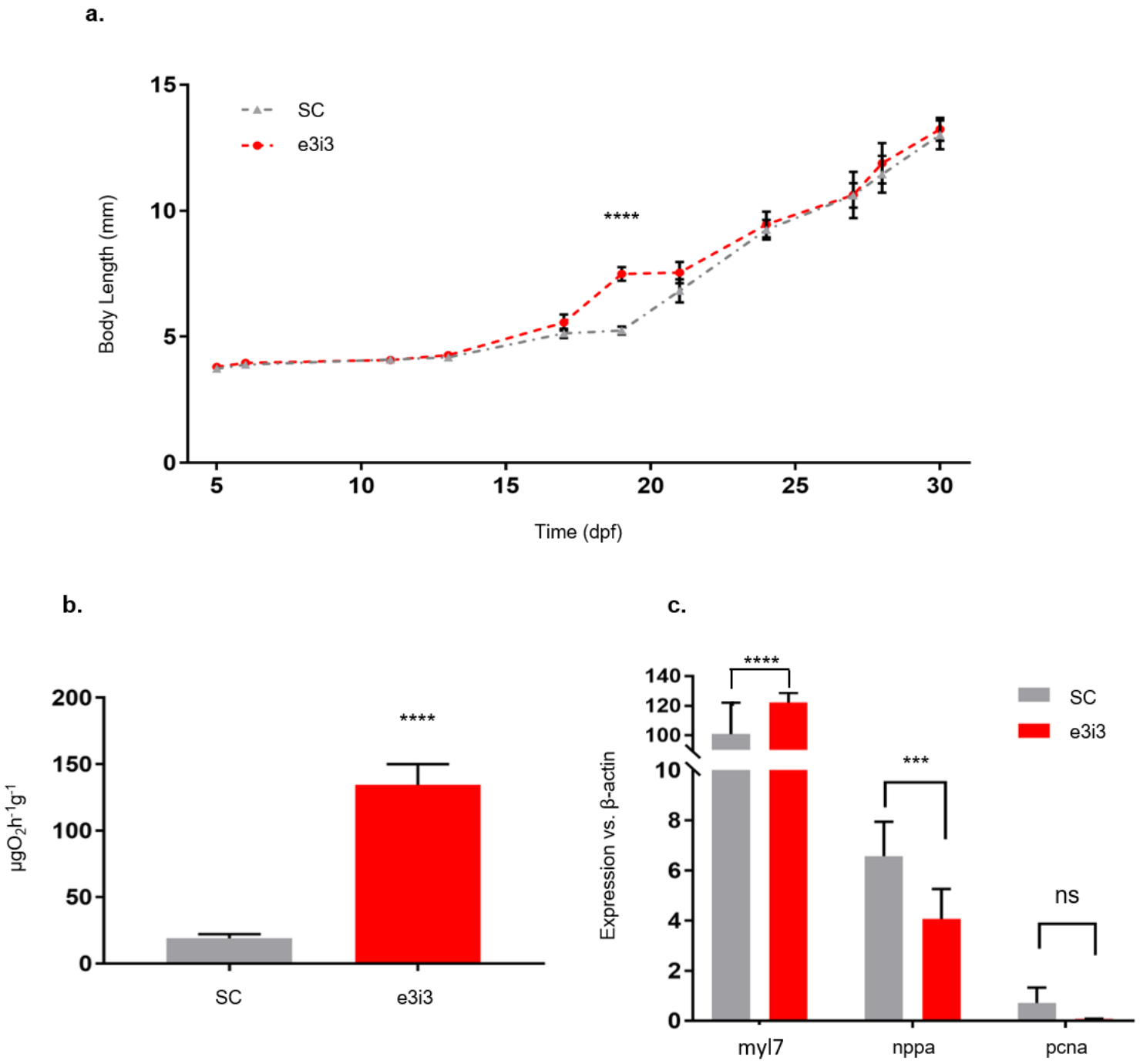

Figure 6 Growth and cardiometabolism continue to be impacted after morpholino attenuation*. 6a.** Mean total body length ± SEM of SC and KD zebrafish up to 30 dpf. Following the embryonic growth spurt, KD zebrafish experienced an additional period of rapid growth between 15 and 20 dpf (*<0.0001). ***6b.*** Mean oxygen consumption + SEM of 30 dpf zebrafish (n=5), adjusted for body weight. KD zebrafish consumed significantly more oxygen per hour per gram of tissue than SC zebrafish (****<0.0001). ***6c***. qPCR results of three genes associated with cardiac performance in adult cardiac tissue, relative to β-actin. *Myl7* expression was significantly elevated in KD zebrafish (****<0.0001) while *nppa* expression was significantly down regulated (***=0.0012) compared to SC zebrafish. There was no significant difference between the expression of *pcna* (p=0.3041). All comparisons by unpaired t-test.

549 **Discussion**

550 The first key finding from this study is that grb10a regulates embryonic growth in zebrafish,
551 consistent with its role in mammalian embryogenesis (47–49). Embryonic body length was
552 significantly elevated in KD zebrafish, and significantly repressed following *grb10a*
553 overexpression, clearly demonstrating the role of grb10a as a modulator of embryonic
554 growth. In addition, key elements in the insulin signalling pathway were significantly
555 upregulated following *grb10a* KD, consistent with the role of grb10a as a negative regulator
556 of this pathway (50,51). Transient disruption of grb10a signalling was sufficient to induce
557 morphological, physiological, and transcriptomic changes which persisted to the late-juvenile
558 stage, despite no further manipulation to the organism. E3i3 treated zebrafish were
559 significantly larger during embryonic development, with significantly elevated metabolic rate,
560 and depressed heart rate. This suggests a clear link between embryonic growth, metabolism,
561 and cardiac phenotype, indicating that grb10a may play a fundamental role in coordinating
562 these distinct pathways.

563 Additionally, metabolic rate remained elevated in the juvenile zebrafish, supporting the
564 concept that disruptions to embryonic growth and development have a lasting impact on
565 health and disease. Both embryonic and adult cardiac systems were impacted by *grb10a* KD.
566 The ability of grb10a disruption to modify growth, metabolism, and cardiac phenotype
567 supports a fundamental link between these three distinct aspects. As gene expression
568 remained significantly perturbed by 30 dpf, it is clear that transient g*rb10a* KD has persistent
569 long-term impacts following attenuation of the morpholino, potentially indicating a lasting
570 epigenetic remodelling. This is the only study to our knowledge to report this impact.

571 Transcriptomic data analysis not only confirmed a prolonged impact of transient KD,
572 persisting after morpholino attenuation, but also revealed important gene expression trends
573 regarding life history phase transitions in WT zebrafish. Two key transitionary phases (5 to 10
574 dpf and 15 to 20 dpf) were identified, with WT zebrafish undergoing a transcriptomic shift
575 between three distinct gene clusters. These clusters correlate with the transition between
576 larval and juvenile phases. Further investigation into these clusters will provide insight into
577 the major factors regulating early growth and development compared to later life
578 homeostasis.

579 In contrast, KD zebrafish only displayed one transitionary phase, indicating grb10a may
580 coordinate this life-history phase transition. There was no clear transition in gene expression
581 between 5 and 10 dpf. This suggests falling levels of grb10a (post 48 hpf peak) in WT zebrafish
582 may induce this gene expression transition, and ablation of this grb10a gradient is sufficient
583 to persistently remodel gene expression and to impact cardiometabolic function in later life.

584 Hypernetwork analysis allowed quantification of the coordination of expression within the
585 transcriptome. There was an increase in connectivity in the hypernetwork model of KD
586 transcriptome activity compared to controls, indicating a greater degree of interaction
587 between age-related genes in the KD zebrafish. The hypernetwork entropy in age-related
588 genes compared with randomly selected genes was reduced to a greater extent in the SC than
589 the KD. A reduction in interactome entropy, as seen in SC zebrafish, is associated with more
590 highly differentiated cell populations, corresponding to narrower biological function (36).
591 Therefore, in KD zebrafish there will be a broader range of biological functions consistent with
592 the increase in connectivity in the hypernetwork. In previous work looking at prepubertal
593 growth in children we noted that greater entropy in growth hormone secretion was
594 associated with better growth (37); these results imply that a broad range of pathways would
595 be contributing to the increased growth hormone secretion.

596 The co-ordination between age-related gene expression and the wider transcriptome was
597 assessed by measuring all genes correlated with the hypernetwork cluster (Galois
598 correspondence). This revealed a 27.8-fold increase in co-ordinated genes in the KD zebrafish
599 compared with SC zebrafish, and highlighted a range of associated pathways. This included
600 cardiovascular development and metabolism in the KD, compared to immunological and
601 growth-associated pathways in the SC. Taken together, these data indicate an ongoing impact
602 of *grb10a* KD on biological functions.

603 Findings from this study may also provide important insight for the agri- and aquaculture
604 industries. Embryonic heart rate was significantly depressed in KD zebrafish embryos, despite
605 increased body length, indicating increased cardiac efficiency over SC individuals. Myl7
606 expression, a cardiac specific myosin light chain protein, was upregulated in the mature KD
607 cardiac tissue, while pcna, a marker of proliferation, was not significantly different between
608 the two groups. This suggests the difference in myl7 gene expression is due to an increase in
609 cardiac cell size (hypertrophy) rather than cell number (hyperplasia).

610 In addition, the promotion of embryonic growth induced by *grb10a* KD may be a key
611 alternative to growth hormone treatment for improving meat yield and production efficiency.
612 This may be particularly useful for fisheries, as larger juvenile fish will be more capable of
613 overwintering (52,53), and thus improve fish stocks.

614 Cardiac development was also linked to the persistent changes observed in the transcriptome
615 in the KD animals. The previously described molecular cardiac phenotype markers, while not
616 present in the clusters of genes showing persistent dysregulation, were shown to display
617 altered age-related expression in early life. This suggests an indirect action on later life cardiac
618 physiology.

619 Finally, this model of embryonic growth perturbation may yield significant insights into the
620 propensity for early growth disruption in SGA and LGA new-borns to convey elevated risk of
621 disease in later life. It is widely accepted that many disorders may have their origins during
622 embryonic development (often termed the developmental origins of adult disease hypothesis
623 (54)). Early life growth disruption and non-average for gestational age status convey elevated
624 risk of cardiac and metabolic disorders in later life (1,55–57). While this has been observed
625 across multiple human populations (3,58,59), the mechanisms involved are not fully
626 understood. As grb10a modulation is sufficient to alter embryonic growth trajectory,
627 metabolic rate, and cardiac function, this model may prove key in understanding the
628 mechanisms involved in the developmental origins of health and disease and identifying novel
629 avenues for prevention and treatment.

630 While mammalian models have been used to show the immediate impact of embryonic
631 growth disruption, replicated in this study, their use for longitudinal study is limited, and little
632 research has been conducted into later life impacts of early growth disruption. Due to the
633 nature of human data collection, matched data for embryonic growth rate and later life
634 disease risks is not possible, with measurements limited to mass and body size at birth. While
635 this is somewhat informative, multiple distinct growth trajectories may yield similar birth
636 weights, such as growth restriction followed by catch-up growth, or overgrowth followed by
637 catch-down growth (55). Both catch-up and catch-down growth have been reported to
638 correlate with increased risk of chronic health disorders (1,60,61). Furthermore, the growth
639 profile was shifted to an earlier age in the KD zebrafish, reflecting similar growth profiles
640 observed in cases of precocious puberty (62). This suggests the KD zebrafish may mature at a

641 greater rate than SCs and presents an interesting model for investigating growth and
642 maturation. This model not only facilitates growth rate measurements, but due to the short
643 generation time is also highly suitable for longitudinal study throughout adult life.

644 As key physiological measurements and the transcriptomic landscape is persistently
645 remodelled following transient *grb10a* disruption, this model may provide the link between
646 embryonic development and later disease risk (63). Investigation into the metabolic and
647 cardiac performance of the adult is the next key step.

648 **Conclusion**

649 This study proves transient knockdown of *grb10a* expression alters growth trajectory and
650 cardiometabolic phenotype in embryonic zebrafish. This impact persists into adulthood,
651 correlating with a measurable remodelling of the transcriptomic landscape. This provides
652 significant evidence to suggest grb10a plays a fundamental role in the coordination of these
653 distinct physiological pathways and could represent a promising avenue for production
654 enhancement in an agricultural setting. The novel model of early growth disruption generated
655 in this study, featuring easily measurable phenotypic characteristics, a short developmental
656 window, and rapid generation time, provides much needed groundwork for thorough
657 longitudinal study into the mechanisms underpinning the developmental origins of health and
658 disease.

659 **Acknowledgements**

660 This work was funded by the Biotechnology and Biological Sciences Research Council at the
661 University of Manchester, Manchester, UK, in combination with an unrestricted Merck
662 research grant, Darmstadt, Germany. Preliminary and the transcriptomic work was partially
663 funded by a University of Manchester Research Institute Pump Priming Fund entitled "The
664 quantitative comparison of the Zebrafish as a model of human development in relation to
665 paediatric medicine", RMS 104699.

666 The authors would also like to acknowledge the following people: Dr. Andrew Badrock for his
667 training, guidance, and donation of reagents, and Jack Broadbent and Joseph Whitehead for
668 their preliminary work in quantifying growth and metabolism in this model.

669

670 **Competing Interests**

671 The authors declare the research was conducted in the absence of any conflicts of interest.

672 **Data availability**

673 Transcriptomic data is available from the Gene Expression Omnibus (GSE162474).

674 **References**

675 1. Lei X, Zhao D, Huang L, Luo Z, Zhang J, Yu X, et al. Childhood Health Outcomes in
676 Term, Large-for-Gestational-Age Babies with Different Postnatal Growth Patterns. Am
677 J Epidemiol [Internet]. 2018 Jul 13;187(3):507–14. Available from:
678 https://doi.org/10.1093/aje/kwx271

679 2. Kimm SYS. Fetal origins of adult disease : the Barker hypothesis revisited — 2004.
680 Curr Opin Endocrinol Diabetes. 2004;11(192–196):245–9.

681 3. Barker DJP, Osmond C, Kajantie E, Eriksson JG. Growth and chronic disease: Findings
682 in the Helsinki Birth Cohort. Ann Hum Biol. 2009;36(5):444–58.

683 4. Harding J. The nutritional basis of the fetal origins of adult disease. Int J Epidemiol
684 [Internet]. 2001;30(1):15–23. Available from: https://academic.oup.com/ije/article-
685 lookup/doi/10.1093/ije/30.1.15

686 5. Desbuquois B, Carré N, Burnol A-FF, Carre N, Burnol A-FF. Regulation of insulin and
687 type 1 insulin-like growth factor signaling and action by the Grb10/14 and SH2B1/B2
688 adaptor proteins. FEBS J. 2013 Feb;280(3):794–816.

689 6. Charalambous M, da Rocha ST, Hernandez A, Ferguson-Smith AC. Perturbations to
690 the IGF1 growth pathway and adult energy homeostasis following disruption of
691 mouse chromosome 12 imprinting. Acta Physiol. 2014;210(1):174–87.

692 7. Murdaca J, Treins C, Monthouel-Kartmann M-N, Pontier-Bres R, Kumar S, Van
693 Obberghen E, et al. Grb10 prevents Nedd4-mediated vascular endothelial growth
694 factor receptor-2 degradation. J Biol Chem. 2004 Jun;279(25):26754–61.

695 8. Tezuka N, Brown AMC, Yanagawa S ichi. GRB10 binds to LRP6, the Wnt co-receptor
696 and inhibits canonical Wnt signaling pathway. Biochem Biophys Res Commun

697 [Internet]. 2007 May 11 [cited 2020 Oct 20];356(3):648–54. Available from:
698 https://pubmed.ncbi.nlm.nih.gov/17376403/

699 9. Wick KR, Werner ED, Langlais P, Ramos FJ, Dong LQ, Shoelson SE, et al. Grb10 inhibits
700 insulin-stimulated insulin receptor substrate (IRS)-phosphatidylinositol 3-kinase/Akt
701 signaling pathway by disrupting the association of IRS-1/IRS-2 with the insulin
702 receptor. J Biol Chem. 2003 Mar;278(10):8460–7.

703 10. Charalambous M, Cowley M, Geoghegan F, Smith FM, Radford EJ, Marlow BP, et al.
704 Maternally-inherited Grb10 reduces placental size and efficiency. Dev Biol [Internet].
705 2010 Jan 1 [cited 2017 Nov 6];337(1):1–8. Available from:
706 http://linkinghub.elsevier.com/retrieve/pii/S0012160609012548

707 11. Everson TM, Marable C, Deyssenroth MA, Punshon T, Jackson BP, Lambertini L, et al.
708 Placental expression of imprinted genes, overall and in sex-specific patterns,
709 associated with placental cadmium concentrations and birth size. Environ Health
710 Perspect [Internet]. 2019 May;127(5):57005. Available from:
711 https://pubmed.ncbi.nlm.nih.gov/31082282

712 12. Depetris RS, Hu J, Gimpelevich I, Holt LJ, Daly RJ, Hubbard SR. Structural basis for
713 inhibition of the insulin receptor by the adaptor protein Grb14. Mol Cell [Internet].
714 2005;20(2):325–33. Available from: http://ac.els-cdn.com/S1097276505015984/1-
715 s2.0-S1097276505015984-main.pdf?_tid=11727a1a-b532-11e5-96b1-
716 00000aacb360&acdnat=1452166415_c128af004e062d38d997f991a691a7be

717 13. Crippa M, Bonati MT, Calzari L, Picinelli C, Gervasini C, Sironi A, et al. Molecular
718 Etiology Disclosed by Array CGH in Patients With Silver-Russell Syndrome or Similar
719 Phenotypes. Front Genet [Internet]. 2019 Oct 15;10:955. Available from:
720 https://pubmed.ncbi.nlm.nih.gov/31749829

721 14. Clayton P, Chatelain P, Tato L, Yoo HW, Ambler GR, Belgorosky A, et al. A
722 pharmacogenomic approach to the treatment of children with GH deficiency or
723 Turner syndrome. Eur J Endocrinol. 2013 Sep;169(3):277–89.

724 15. De Leonibus C, Murray P, Garner T, Hanson D, Clayton P, Stevens A. The in vitro
725 functional analysis of single-nucleotide polymorphisms associated with growth

726 hormone (GH) response in children with GH deficiency. Pharmacogenomics J
727 [Internet]. 2019 Apr 1 [cited 2020 Oct 12];19(2):200–10. Available from:
728 https://www.nature.com/articles/s41397-018-0026-4

729 16. De Leonibus C, Chatelain P, Knight C, Clayton P, Stevens a. Effect of summer daylight
730 exposure and genetic background on growth in growth hormone-deficient children.
731 Pharmacogenomics J [Internet]. 2016;16(6):540–50. Available from:
732 http://www.nature.com/doifinder/10.1038/tpj.2015.67

733 17. Calkins K, Devaskar SU, Angeles L. Fetal Origins of Adult Disease. Curr Probl Pediatr
734 Adolesc Heal Care. 2011;41(6):158–76.

735 18. Robinson R. The fetal origins of adult disease: No longer just a hypothesis and may be
736 critically important in south Asia. BMJ. 2001;322(7283):375–6.

737 19. Barker DJP, Martyn CN. The maternal and fetal origins of cardiovascular disease. J
738 Epidemiol Community Heal. 1992;46:8–11.

739 20. Sun Y, Liu Y, Sun X, Lin Y, Yin D, Xu S, et al. Insights into body size variation in
740 cetaceans from the evolution of body-size-related genes. BMC Evol Biol [Internet].
741 2019 Jul 27;19(1):157. Available from: https://pubmed.ncbi.nlm.nih.gov/31351448

742 21. Xu L, Yang L, Wang L, Zhu B, Chen Y, Gao H, et al. Probe-based association analysis
743 identifies several deletions associated with average daily gain in beef cattle. BMC
744 Genomics [Internet]. 2019 Jan 10;20(1):31. Available from:
745 https://pubmed.ncbi.nlm.nih.gov/30630414

746 22. Magee DA, Sikora KM, Berkowicz EW, Berry DP, Howard DJ, Mullen MP, et al. DNA
747 sequence polymorphisms in a panel of eight candidate bovine imprinted genes and
748 their association with performance traits in Irish Holstein-Friesian cattle. BMC Genet
749 [Internet]. 2010 Oct 13;11:93. Available from:
750 https://pubmed.ncbi.nlm.nih.gov/20942903

751 23. Smith FM, Garfield AS, Ward A. Regulation of growth and metabolism by imprinted
752 genes. Cytogenet Genome Res. 2006;113(1–4):279–91.

753 24. Charalambous M, Smith FM, Bennett WR, Crew TE, Mackenzie F, Ward A. Disruption

754 of the imprinted Grb10 gene leads to disproportionate overgrowth by an Igf2-
755 independent mechanism. Proc Natl Acad Sci U S A. 2003 Jul;100(14):8292–7.

756 25. Stainier DYR, Raz E, Lawson ND, Ekker SC, Burdine RD, Eisen JS, et al. Guidelines for
757 morpholino use in zebrafish. PLoS Genet. 2017;13(10).

758 26. Ye J, Coulouris G, Zaretskaya I, Cutcutache I, Rozen S, Madden TL. Primer-BLAST: a
759 tool to design target-specific primers for polymerase chain reaction. BMC
760 Bioinformatics. 2012 Jun;13:134.

761 27. Schindelin J, Arganda-Carreras I, Frise E, Kaynig V, Longair M, Pietzsch T, et al. Fiji: An
762 open-source platform for biological-image analysis. Nat Methods [Internet]. 2012 Jun
763 28;9(7):676–82. Available from: https://www.ncbi.nlm.nih.gov/pubmed/22743772

764 28. Fink M, Flekna G, Ludwig A, Heimbucher T, Czerny T. Improved translation efficiency
765 of injected mRNA during early embryonic development. Dev Dyn an Off Publ Am
766 Assoc Anat. 2006;235(12):3370–8.

767 29. Avey SR, Ojehomon M, Dawson JF, Gillis TE. How the expression of green fluorescent
768 protein and human cardiac actin in the heart influences cardiac function and aerobic
769 performance in zebrafish danio rerio. J Fish Biol [Internet]. 2018 Jan 1 [cited 2020 Oct
770 15];92(1):177–89. Available from: https://pubmed.ncbi.nlm.nih.gov/29194605/

771 30. SigmaAldrich. Assay Optimization and Validation A Technical Guide to PCR
772 Technologies Table of Contents [Internet]. MERCK. 2015 [cited 2020 Mar 1]. p. 1–11.
773 Available from: https://www.sigmaaldrich.com/technical-
774 documents/articles/biology/assay-optimization-and-validation.html#validating

775 31. Durinck S, Spellman PT, Birney E, Huber W. Mapping identifiers for the integration of
776 genomic datasets with the R/ Bioconductor package biomaRt. Nat Protoc [Internet].
777 2009 [cited 2020 Sep 8];4(8):1184–91. Available from:
778 /pmc/articles/PMC3159387/?report=abstract

779 32. Fontes M, Soneson C. The projection score - an evaluation criterion for variable
780 subset selection in PCA visualization. BMC Bioinformatics [Internet]. 2011;12(1):307.
781 Available from: https://doi.org/10.1186/1471-2105-12-307

782 33. Battiston F, Cencetti G, Iacopini I, Latora V, Lucas M, Patania A, et al. Networks
783 beyond pairwise interactions: Structure and dynamics. Physics Reports. Elsevier B.V.;
784 2020.

785 34. Zhang B, Horvath S. A general framework for weighted gene co-expression network
786 analysis. Stat Appl Genet Mol Biol [Internet]. 2005 Aug 12 [cited 2020 Sep 8];4(1).
787 Available from: https://pubmed.ncbi.nlm.nih.gov/16646834/

788 35. Luo F, Yang Y, Chen CF, Chang R, Zhou J, Scheuermann RH. Modular organization of
789 protein interaction networks. Bioinformatics [Internet]. 2007 Jan 15 [cited 2020 Sep
790 8];23(2):207–14. Available from:
791 https://academic.oup.com/bioinformatics/article/23/2/207/204437

792 36. Banerji CRS, Miranda-Saavedra D, Severini S, Widschwendter M, Enver T, Zhou JX, et
793 al. Cellular network entropy as the energy potential in Waddington's differentiation
794 landscape. Sci Rep [Internet]. 2013 Oct 24 [cited 2020 Aug 28];3(1):1–7. Available
795 from: www.nature.com/scientificreports

796 37. Gill MS, Tillmann V, Veldhuis JD, Clayton PE. Patterns of GH Output and Their
797 Synchrony with Short-Term Height Increments Influence Stature and Growth
798 Performance in Normal Children. J Clin Endocrinol Metab [Internet]. 2001 Dec 1 [cited
799 2020 Oct 20];86(12):5860–3. Available from: https://academic.oup.com/jcem/article-
800 lookup/doi/10.1210/jcem.86.12.8116

801 38. Zhang JD, Hatje K, Sturm G, Broger C, Ebeling M, Burtin M, et al. Detect tissue
802 heterogeneity in gene expression data with BioQC. BMC Genomics [Internet]. 2017
803 Apr 4 [cited 2020 Sep 8];18(1):277. Available from:
804 http://bmcgenomics.biomedcentral.com/articles/10.1186/s12864-017-3661-2

805 39. Subramanian A, Tamayo P, Mootha VK, Mukherjee S, Ebert BL, Gillette MA, et al.
806 Gene set enrichment analysis: A knowledge-based approach for interpreting genome-
807 wide expression profiles. Proc Natl Acad Sci U S A [Internet]. 2005 Oct 25 [cited 2020
808 Aug 28];102(43):15545–50. Available from:
809 www.pnas.orgcgidoi10.1073pnas.0506580102

810 40. Liao Y, Wang J, Jaehnig EJ, Shi Z, Zhang B. WebGestalt 2019: gene set analysis toolkit

811 with revamped UIs and APIs. Nucleic Acids Res [Internet]. 2019 Jul 1 [cited 2020 Aug
812 28];47(W1):W199–205. Available from: http://www.webgestalt.org.

813 41. Liberzon A, Birger C, Thorvaldsdóttir H, Ghandi M, Mesirov JP, Tamayo P. The
814 Molecular Signatures Database Hallmark Gene Set Collection. Cell Syst [Internet].
815 2015 Dec 23 [cited 2020 Sep 8];1(6):417–25. Available from:
816 http://dx.doi.org/10.1016/j.cels.2015.12.004http://dx.doi.org/10.1016/j.cels.2015.12
817 .004

818 42. Package "ggpubr" Type Package Title "ggplot2" Based Publication Ready Plots
819 [Internet]. 2020 [cited 2020 Sep 8]. Available from:
820 https://rpkgs.datanovia.com/ggpubr/

821 43. Benjamini Y, Hochberg Y. Controlling the False Discovery Rate: A Practical and
822 Powerful Approach to Multiple Testing. Vol. 57, Source: Journal of the Royal
823 Statistical Society. Series B (Methodological). 1995.

824 44. Motulsky H, Brown R. Detecting outliers when fitting data with nonlinear regression -
825 a new method based on robust nonlinear regression and the false discovery rate.
826 BMC Bioinformatics [Internet]. 2006;7(123). Available from:
827 http://www.biomedcentral.com/1471-2105/7/123

828 45. Banerji CRS, Severini S, Teschendorff AE. Network transfer entropy and metric space
829 for causality inference. Phys Rev E - Stat Nonlinear, Soft Matter Phys [Internet]. 2013
830 May 31 [cited 2020 Aug 28];87(5):052814. Available from:
831 https://journals.aps.org/pre/abstract/10.1103/PhysRevE.87.052814

832 46. Cheng C, Liu H, Tan C, Tong D, Zhao Y, Liu X, et al. Mutation in NPPA causes atrial
833 fibrillation by activating inflammation and cardiac fibrosis in a knock-in rat model.
834 FASEB J [Internet]. 2019 Aug 1 [cited 2020 Oct 12];33(8):8878–91. Available from:
835 https://pubmed.ncbi.nlm.nih.gov/31034774/

836 47. Riedel H. Grb10 exceeding the boundaries of a common signaling adapter. Front
837 Biosci. 2004 Jan;9(JAN):603–18.

838 48. Shiura H, Miyoshi N, Konishi A, Wakisaka-Saito N, Suzuki R, Muguruma K, et al.
839 Meg1/Grb10 overexpression causes postnatal growth retardation and insulin

840 resistance via negative modulation of the IGF1R and IR cascades. Biochem Biophys
841 Res Commun. 2005 Apr;329(3):909–16.

842 49. Holt LJ, Brandon AE, Small L, Suryana E, Preston E, Wilks D, et al. Ablation of Grb10
843 Specifically in Muscle Impacts Muscle Size and Glucose Metabolism in Mice.
844 Endocrinology. 2018;159(3):1339–51.

845 50. Dufresne AM, Smith RJ. The adapter protein GRB10 is an endogenous negative
846 regulator of insulin-like growth factor signaling. Endocrinology. 2005
847 Oct;146(10):4399–409.

848 51. Mori K, Giovannone B, Smith RJ. Distinct Grb10 domain requirements for effects on
849 glucose uptake and insulin signaling. Mol Cell Endocrinol. 2005;230(1–2):39–50.

850 52. Francová K, Ondračková M. Overwinter Body Condition, Mortality and Parasite
851 Infection in Two Size Classes of 0+ Year Juvenile European Bitterling Rhodeus Amarus.
852 J Fish Biol. 2013;82(2):555–68.

853 53. Shoup D, Wahl D. Body Size, Food, and Temperature Affect Overwinter Survival of
854 Age-0 Bluegills. Trans Am Fish Soc. 2011;140(5):1298–304.

855 54. Barker DJ. The fetal and infant origins of adult disease. BMJ. 1990;301(6761):1111.

856 55. Godfrey KM, Inskip HM, Hanson MA. The long-term effects of prenatal development
857 on growth and metabolism. Semin Reprod Med. 2011;29(3):257–65.

858 56. Devaskar SU, Chu A. Intrauterine growth restriction: Hungry for an answer.
859 Physiology. 2016 Feb 17;31(2):131–46.

860 57. Jaquet D, Gaboriau A, Czernichow P, Levy-Marchal C. Insulin Resistance Early in
861 Adulthood in Subjects Born with Intrauterine Growth Retardation [1]. J Clin Endocrinol
862 Metab [Internet]. 2000;85(4):1401–6. Available from:
863 https://academic.oup.com/jcem/article-lookup/doi/10.1210/jcem.85.4.6544

864 58. Savanur MS, Ghugre PS. BMI, body fat and waist-to-height ratio of stunted v. non-
865 stunted Indian children: A case-control study. Public Health Nutr [Internet].
866 2016/02/19. 2016;19(8):1389–96. Available from:
867 https://www.cambridge.org/core/article/bmi-body-fat-and-waisttoheight-ratio-of-

868 stunted-v-nonstunted-indian-children-a-casecontrol-
869 study/3B83DFA36072ED691FC09FF3B2068D2F

870 59. Painter RC, Osmond C, Gluckman P, Hanson M, Phillips DIW, Roseboom TJ.
871 Transgenerational effects of prenatal exposure to the Dutch famine on neonatal
872 adiposity and health in later life. BJOG An Int J Obstet Gynaecol. 2008;115(10):1243–
873 9.

874 60. Finkielstain GP, Lui JC, Baron J. Catch-up growth: Cellular and molecular mechanisms.
875 World Rev Nutr Diet. 2013;106:100–4.

876 61. Singhal A. Long-Term Adverse Effects of Early Growth Acceleration or Catch-Up
877 Growth. Vol. 70, Annals of Nutrition and Metabolism. 2017. p. 236–40.

878 62. Tirumuru SS, Arya P, Latthe P, Kirk J. Understanding precocious puberty in girls.
879 Obstet Gynaecol [Internet]. 2012 Apr 1 [cited 2020 Oct 20];14(2):121–9. Available
880 from: http://doi.wiley.com/10.1111/j.1744-4667.2012.00094.x

881 63. Turan N, Ghalwash MF, Katari S, Coutifaris C, Obradovic Z, Sapienza C. DNA
882 methylation differences at growth related genes correlate with birth weight : a
883 molecular signature linked to developmental origins of adult disease ? BMC Med
884 Genomics [Internet]. 2012;5(1):10. Available from:
885 http://www.biomedcentral.com/1755-8794/5/10

886 **Tables**

887 **Table 1. Oligonucleotide sequences**

A) Morpholino-modified antisense oligonucleotides			
Name	**Accession no.**	**Sequence**	
e3i3	BX571825	CATACAGTATGCATTACCTGACAGC	
e4i4		GTGTCTGTTTTCAGCTCTTACATGT	
Standard Control		CCTCTTACCTCAGTTACAATTTATA	
B) Primers for cloning *grb10a* cDNA and for validating splicing interruption			
Name	**Accession no.**	**Forward**	**Reverse**
grb10a cDNA	NM_0010042	gacagaatcgatGACTGAGTATGGC	gacagatctagaTCATAAGGCC
grb10a exon3-	BX571825	TGGTGAATGACATGGCCTCT	CTGCATGGTCAAGACACAC
grb10a exon3-		TGGTGAATGACATGGCCTCT	CTGACGGATAATAGCTACA
B) Primers for qPCR			
Gene	**Accession no.**	**Forward**	**Reverse**
grb10a	NM_0010042	TGGATGACTGCTTTTAGACTGC	CGACCAGTCCTTCCAGAAA
actb1	NM_131031.	CTTCCAGCAGATGTGGATCA	GCCATTTAAGGTGGCAACA
myl7	NM_131329.	TCACTGTCTTCCTCACCCTC	CACGTCTATTGGAGCCACT
pcna	NM_131404.	AGGCAACATCAAGCTCTCAC	ATTTGACGTGTCCCATGTCT
nppa	NM_198800.	AAGCAAAAGCTTGTCTGG	ACTGTATCCGCGTATTGCA

888 **Table 2. Microinjection Solutions**

Injection	**Oligonucleotide**	**nCerulean**	**Phenol Red**
Standard Control (5	0.5 mM human beta globin morpholino	50 ng/µl	1 µl
grb10a KD (5 µl)	0.5 mM e3i3 or e4i4 morpholino	50 ng/µl	1 µl
grb10a OE (5 µl)	500 ng/µl *grb10a* RNA	50 ng/µl	1 µl

889 **Table 3. Thermocycling Parameters**

Procedure	**Temperature (°C)**	**Time (S)**	**Cycles**
NEB Q5 Hot Start	95	300	
	95	30	35
	55	30	
	72	120	
	72	600	
NEB Taq	95	30	
	95	15	30
	55	15	
	68	30	
	68	300	
SyBr Green qPCR	95	30	
	95	5	40
	51	15	
	72	10	

890 **Table 4. Western Blot Antibodies**

Target	Species	Supplier	Dilution
AKT	Mouse	Cell Signalling #2920	1:1000
p-AKT	Rabbit	Cell Signalling - #5831	1:1000
ERK1/2	Mouse	Santa Cruz Biotechnology sc-135900	1:1000
p-ERK1/2	Rabbit	Cell Signalling #4370	1:1000
S6	Mouse	Cell Signalling - #2317	1:1000
p-S6	Rabbit	Cell Signalling - #2215	1:1000
Anti-Mouse HRP linked IgG	Horse	Cell Signalling - #7076	1:5000
Anti-Rabbit HRP linked IgG	Goat	Cell Signalling - #7074	1:5000

891

892 **Supplementary Figures**

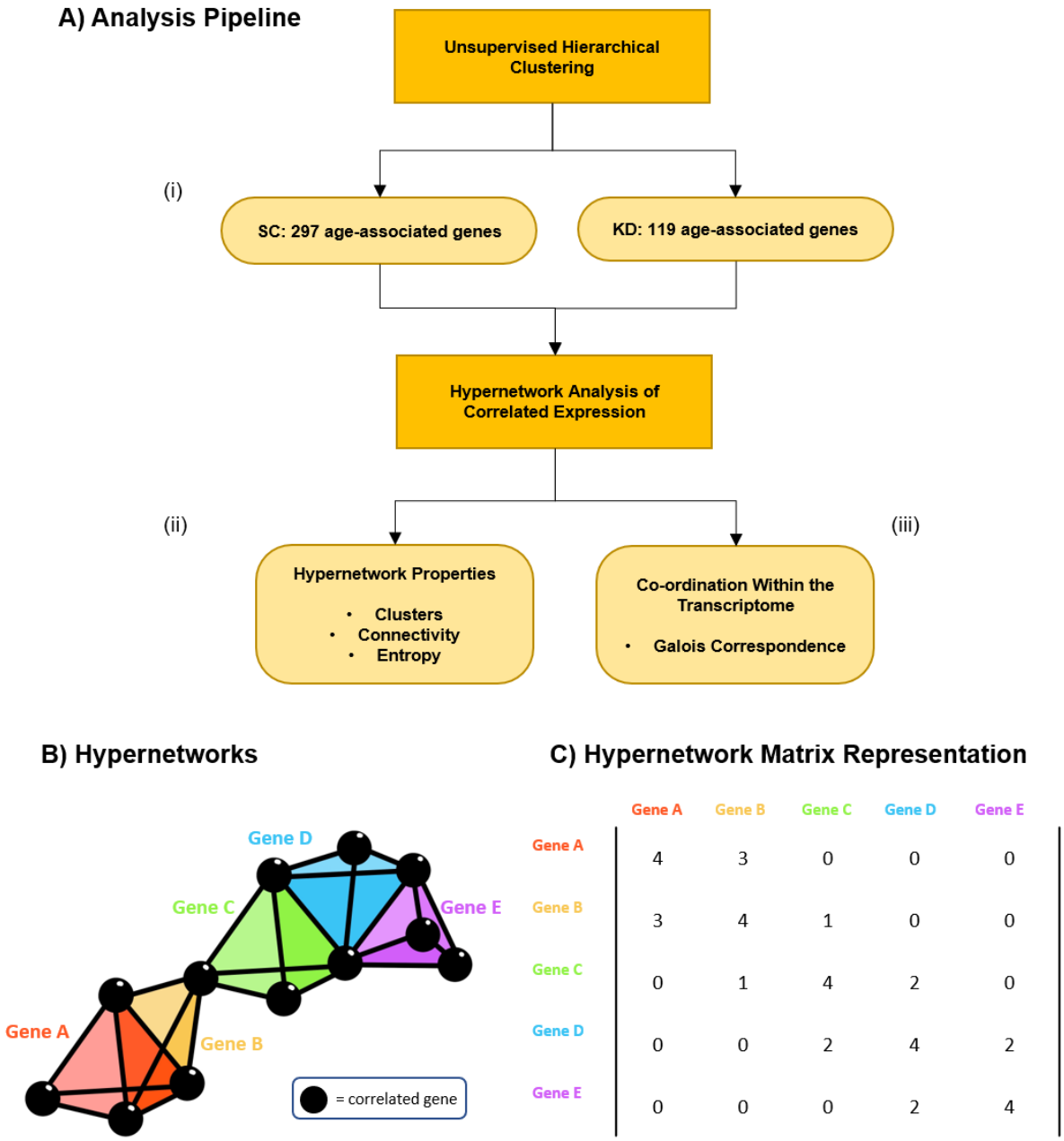

893 ***Supplementary Figure 1. Pipeline of transcriptomic analysis and hypernetworks. 1a.*** Analysis pipeline of
894 transcriptomic data. **(i)** Unsupervised hierarchical clustering was performed using a projection score to capture
895 the most informative age-associated gene clustering in principal component analysis under a variance strip.
896 Hypernetwork analysis was generated using the age associated genes identified in both SC and KD animals. **(ii)**
897 Hypernetworks were quantified by comparing cluster structure, connectivity, and entropy. **(iii)** The impact of co-
898 ordinated gene expression on the whole transcriptome was measured by identifying the Galois correspondence
899 within the hypernetwork. 1***b.*** A general model of a hypernetwork, shown as a three dimensional representation
900 of genes (coloured tetrahedra) correlating with the expression of four other genes (black spheres). Shared
901 correlations are represented by matching vertices, edges, and faces of the tetrahedra. ***1c.*** A hypernetwork
902 representation of the "higher order" interactions within the transcriptome. This summary of the genes with
903 shared correlations can be considered as an incidence matrix of a multi-dimensional network.

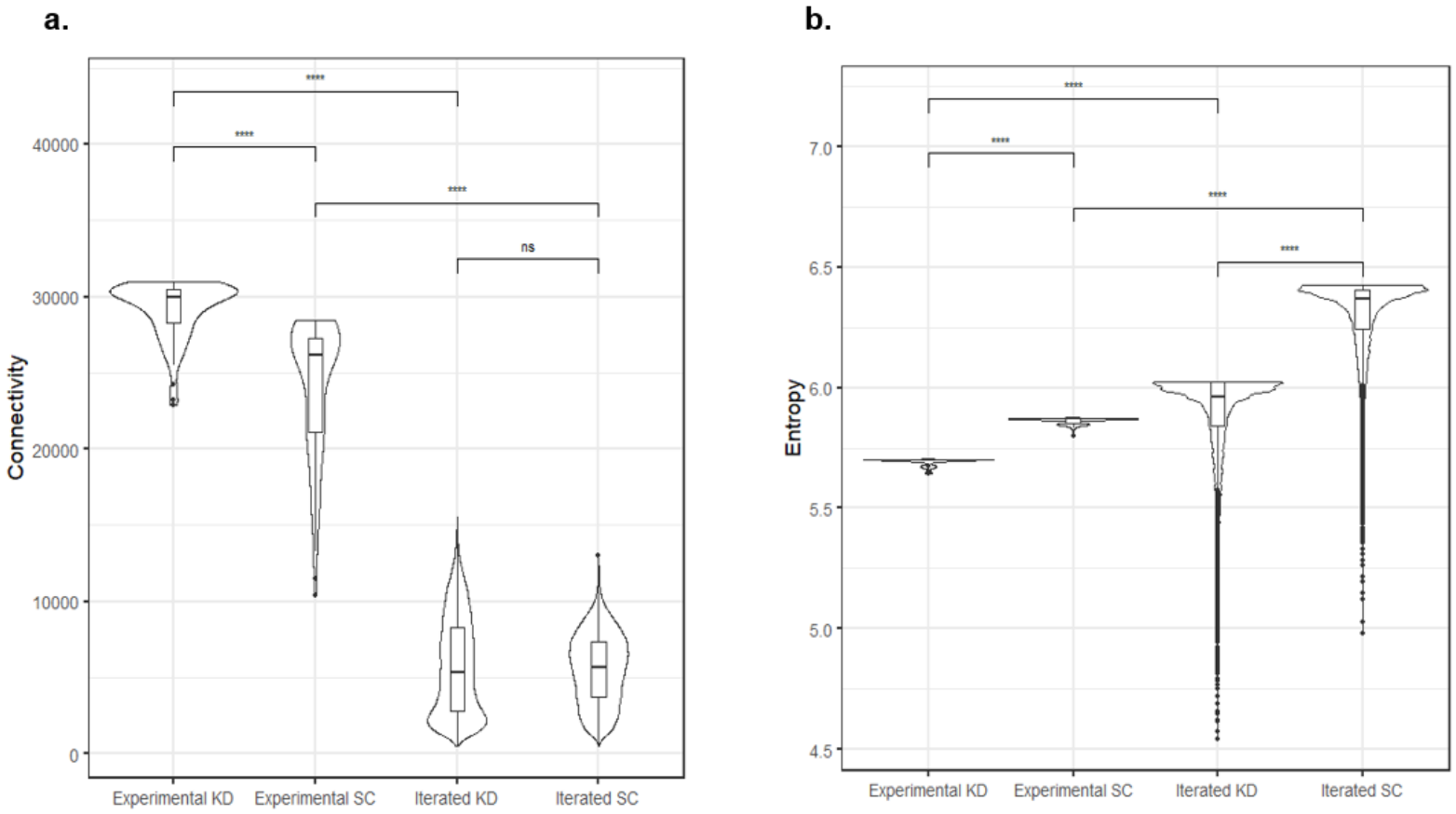

904 ***Supplementary Figure 2. Connectivity (left) and entropy (right) of 20-30 dpf associated genes in the SC and KD***
905 ***zebrafish compared with randomly selected gene sets.*** 2***a.*** Connectivity in the experimental data was
906 significantly greater than in the random iterative data, and greater in the KD data than SC (p<0.0001). 2***b.*** Entropy
907 was significantly lower in the experimental data than the random iterative data. Entropy was lower in the KD
908 than SC, though the reduction in entropy between the experimental data and interated data was greater in the
909 SC than the KD.

910

911

912

913

914

915

916

917

918

919

920 **Supplementary Tables**

921 ***Supplementary Table 1*.** Gene set enrichment analysis on age related gene expression in KD
922 and SC zebrafish. 75212 probe ids mapped to 3733 human orthologues. Probe sets were
923 collapsed to gene summary by averaging and group ANOVAs were performed by age groups.
924 Q-values are reported as the false discovery rate modified p-value of the GSEA, performed in
925 Qlucore Omics Explorer (v3.6) using Gene Ontology Biological Process pathways.

926 ***Supplementary Table 2*.** 12775 and 459 genes defined by the Galois correspondence from the
927 20-30 dpf KD and SC hypernetwork clusters respectively, together with rank regression scores
928 and p-values. Zebrafish gene symbol and corresponding human orthologue shown.

929 ***Supplementary Table 3*.** A subset of 3460 genes from the Galois correspondence showing
930 fluctuating gene expression from 15 to 30 dpf and associating with metabolism and
931 development gene ontology pathways. Displayed as zebrafish gene symbols, corresponding
932 human orthologues, R-statistics of age rank regression analysis, and p-values.

933 ***Supplementary Table 4*.** Dysregulated expression of cardiac phenotype marker genes in the
934 KD zebrafish. False discovery rate modified p-value (q-value) shown for age group ANOVA.